RECENT CONTRIBUTIONS ON MICROCALORIMETER RESEARCH

S.H. MOSELEY, R.L. KELLEY, C.K. STAHLE,
M.D. AUDLEY, A.E. SZYMKOWIAK, AND G. MADEJSKI

LABORATORY FOR HIGH ENERGY
ASTROPHYSICS

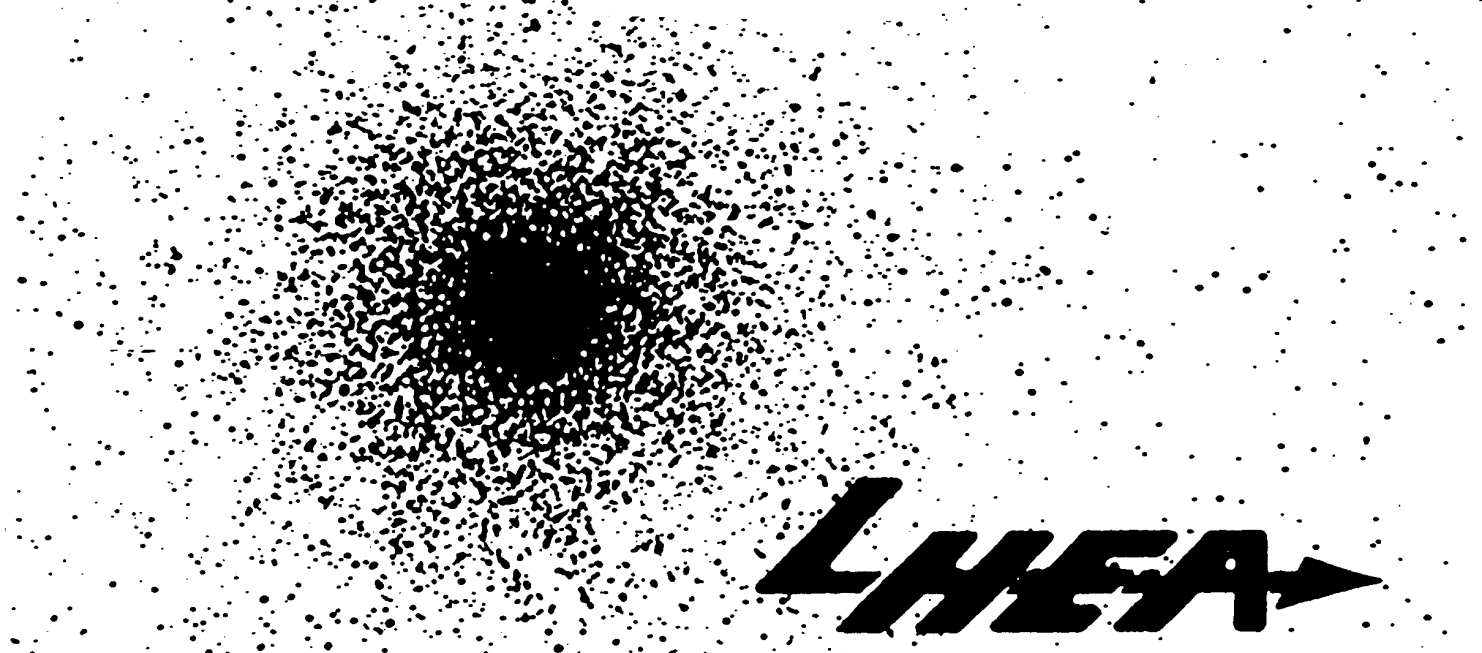

National Aeronautics And Space Administration
Goddard Space Flight Center
Greenbelt, Maryland 20771

93-78

RECENT CONTRIBUTIONS ON MICROCALORIMETER RESEARCH

S.H. MOSELEY[1], R.L. KELLEY, C.K. STAHLE[2],
M.D. AUDLEY[3], A.E. SZYMKOWIAK, and G. MADEJSKI[4]

Code 666
X-ray Astrophysics Branch
Laboratory for High Energy Astrophysics
NASA/Goddard Space Flight Center
Greenbelt, Maryland 20771 USA

[1]Code 685
[2]NAS/NRC Resident Research Associate
[3]Also University of Maryland
[4]Universities Space Research Association

TABLE OF CONTENTS

X-RAY MICROCALORIMETERS - PRINCIPLES AND PERFORMANCE

S. H. Moseley[1], M. Juda[2], R. L. Kelley[1], D. McCammon[2], C. K. Stahle[1,3], A. E. Szymkowiak[1], and J. Zhang[2]

[1]NASA / Goddard Space Flight Center; [2]Dept. of Physics, University of Wisconsin; [3]NAS/NRC Resident Research Associate

ABSTRACT

Microcalorimeters operating at cryogenic temperatures can be excellent X-ray spectrometers. They simultaneously offer very high spectral resolving power and high efficiency. These attributes are important for X-ray astronomy where most sources have low fluxes, and where high spectral resolution is essential for understanding the physics of the emitting regions. We review the principles of operation of these detectors, limits to their sensitivity, design considerations, techniques of fabrication, and their performance as X-ray spectrometers.

Keywords: X-ray spectroscopy, microcalorimeters, cryogenic detectors, X-ray astronomy.

1. INTRODUCTION

X-ray astronomy is characterized by very low photon fluxes, typically less than 1 photon/s/cm^2. This represents a particular challenge for X-ray spectroscopy. We are confronted with complex spectra, containing information concerning elemental composition, ionization state, temperature, and density in plasmas hotter than ~ 10^6 K (Ref. 1). In order to extract this information, high spectral resolution is required and, to measure any but the brightest objects in the sky, high efficiency spectrometers are essential in order to maximize both the number of spectral channels and the number of photons per channel. One of the challenges of modern X-ray astronomy instrumentation is to produce such detectors.

The quantum X-ray microcalorimeter is one solution to this problem of simultaneously achieving high resolving power and efficiency. The detector consists of an X-ray absorber, a thermometer, and a thermal link to a heat sink (Fig. 1). The energy of the X-ray is determined by measuring the temperature rise which results from the absorption of the photon. The temperature rise ΔT following the absorption of the X-ray of energy E in a detector of heat capacity C

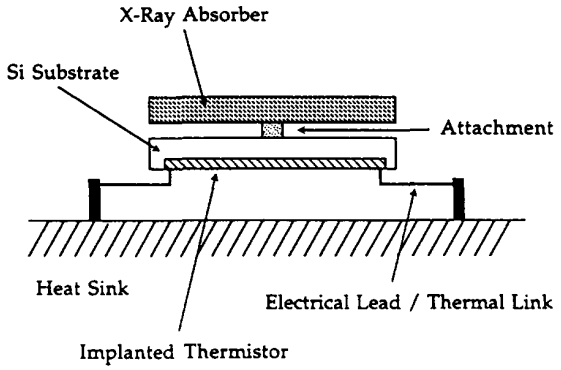

Figure 1. Schematic of microcalorimeter. The X-ray is absorbed and its energy converted to heat in the absorber. The heat flows through the attachment into the detector substrate. The temperature rise of the detector is sensed by a thermometer, which is measured using electrical connections in the thermal links. The detector returns to equilibrium as the heat from the event flows to the heat sink through the thermal links.

is given by

$$\Delta T = \frac{E}{C}. \tag{1}$$

The detector then returns to its heat sink temperature with a time constant

$$\tau = \frac{C}{G}, \tag{2}$$

where G is the thermal conductance between the detector and its heat sink.

For this technique to be successful, all of the photon energy must be converted to heat in a short interval of time. After the absorption and efficient thermalization of the X-ray, the resulting temperature rise must be measured accurately. Since the magnitude of the temperature rise is inversely proportional to the heat capacity of the detector, our goal of high energy resolution dictates that we minimize the overall heat capacity of the detector.

The success of this technique is due in large part to the fact that many materials have extremely low

Proceedings of an ESA Symposium on Photon Detectors for Space Instrumentation, held at ESA/ESTEC, Noordwijk, The Netherlands, 10–12 November 1992. (ESA SP-356, December 1992).

heat capacities at low temperatures. For detectors suitably sized for use with focusing X-ray telescopes, the absorption of a single X-ray photon results in a substantial fractional rise in the temperature of a detector operating at 0.1K. The problem of developing such detectors is essentially one of minimizing its heat capacity given the constraints of detector area, required X-ray absorption efficiency, response time, and thermometer technology. We will describe the limits to the sensitivity of microcalorimeters as X-ray spectrometers, and will discuss the choices which have been made in optimizing the detectors for the X-ray Spectrometer (XRS) on the Advanced X-ray Astrophysics Facility (AXAF).

2. FUNDAMENTALS OF OPERATION AND LIMITS TO SENSITIVITY

2.1 Thermodynamic Limits

The most fundamental limitation to our ability to measure the energy of the X-ray absorbed in a microcalorimeter is set by thermodynamics. The random transport of phonons back and forth in the thermal link between the detector and its heat sink limits our ability to measure the temperature rise due to the absorption of the X-ray (Ref. 2). When combined with the noise of the thermometer, these fluctuations define the achievable energy resolution of a calorimeter. The temperature sensors in our detectors are resistance thermometers and therefore have Johnson noise. Their temperature coefficient α is defined:

$$\alpha = -\frac{d(\log R)}{d(\log T)}. \qquad (3)$$

The thermodynamic limit to the energy resolution of a calorimeter of heat capacity C operated at temperature T with a thermometer of temperature coefficient α has been calculated to be:

$$\Delta E(\mathrm{FWHM}) = 2.35\xi\sqrt{kT^2C}, \qquad (4)$$

where k is Boltzman's constant. The variable ξ decreases with increasing α and is weakly dependent on the temperature dependence of the conductance between the detector and its heat sink (Ref. 2). Since the heat capacities of many of our detector components fall as T^3, the performance of these detectors improves rapidly with decreasing temperature. Initial estimates of resolution predicted that a 1 mm square detector operated at 0.1 K could achieve a resolution of ~1 eV FWHM (Ref. 2). Subsequently, two factors were discovered which have produced higher estimates for practical detectors. They are that the X-rays must be absorbed in a rapidly thermalizing absorber, and that the optimum thermometer size is larger than estimated in Ref. 2. For detectors with areas and absorber thicknesses appropriate for use on XRS, temperatures less than 0.1K are required to achieve the required 10 eV FWHM resolution. At 0.1 K, the predicted thermodynamic limit to resolution for these calorimeters with efficient absorbers is ~4 eV FWHM. The actual resolution achieved with these detectors is ~ 10 eV FWHM, near the thermodynamic limit, and much better than the 130 eV FWHM at 6 keV obtained with Si ionization detectors.

The thermodynamic limit to the energy resolution of the detector improves with increasing temperature coefficient of the thermometer. A higher quality thermometer increases the bandwidth over which the thermal signal can be measured, and hence improves our knowledge of the signal, but only as the square root of the bandwidth (Fig. 2). Work to improve detector performance must focus on the enhancement of thermalization of the X-ray energy and its rapid conduction to the thermometer in order to take advantage of improvements in the thermometer.

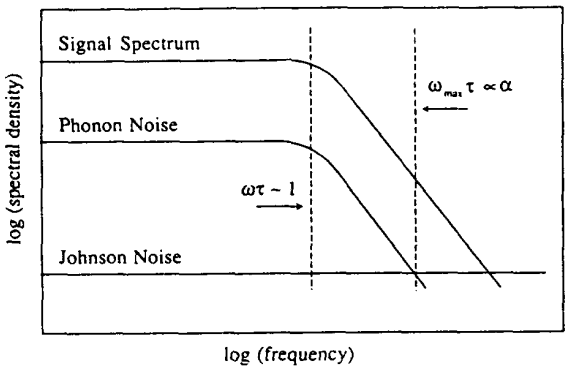

Figure 2. Schematic description of signal and noise in a microcalorimeter. The power spectrum of the temperature change in a detector following the prompt deposition of energy is shown. The signal power is independent of frequency up to the frequency corresponding to the characteristic time constant of the detector and declines to higher frequencies. The phonon noise has the same spectral dependence, so the useful bandwidth of the detector is only limited by the addition of thermometer noise.

2.2 Thermalization of X-ray Energy

The X-ray must be absorbed in a solid in which the energetic excitations created by the absorption of the photon are rapidly and efficiently converted to thermal, or nearly thermal, phonons. This absorber must be of sufficient thickness to absorb the X-rays of interest with high efficiency, but still must have a sufficiently low heat capacity to allow high spectral resolution. Initial work was carried out using Si as the X-ray absorber. It was quickly realized (Ref. 3) that significant amounts of energy were being lost to charge trapping, and that the fraction of total energy lost to trapping varied significantly from event to event, spoiling the resolution of the detector (Fig. 3). Subsequently, experiments showed that several classes of materials thermalize X-ray photons efficiently (Ref. 4). Normal metals, such as Au and Ag are nearly perfect and noiseless X-ray thermalizers. However, their very large free electron specific heats at low temperatures makes them unsuitable for use on practical detectors. Our current materials of choice are zero-gap semimetals (e.g., HgTe) and superconductors (e.g., Sn). In certain forms, these materials have demonstrated efficient and nearly noiseless thermalization, and have sufficiently low heat capacities to make them useful for X-ray astronomy applications.

3. DESIGN CONSIDERATIONS

Much of the early work on X-ray microcalorimeters (Refs. 3,5) was carried out using detectors which were hand-assembled from different components. This is a very flexible approach, but is not conducive to developing devices of the lowest heat capacities. Mass production of highly uniform arrays of such detectors would be difficult.

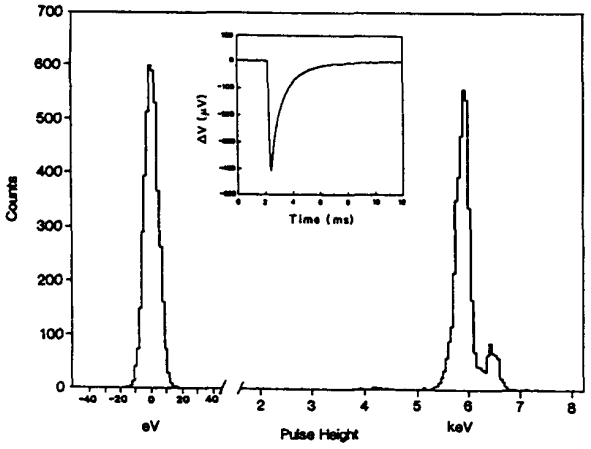

Figure 3. This is the spectrum of the ^{55}Mn X-rays measured in a detector in which the X-rays are absorbed in a high resistivity layer of Si. While each photon is measured with high signal to noise ratio, there is substantial variation in measured pulse height from photon to photon.

To minimize the heat capacity of a detector, including its thermometer, X-ray absorber, and its thermal link and mechanical support, we have developed techniques for fabricating detector arrays by micromachining Si. Silicon has a very low heat capacity and excellent mechanical properties, so it is an excellent choice as a structural material for thermal detectors. The detector body and its thermal links, which provide the structural support, are etched from a single crystal of Si. The thermometer is produced by ion implantation into the Si detector body.

Currently, the absorber, the only non-silicon element in the detector, is attached to the micromachined detector body by an epoxy joint (Fig. 4). This joint provides mechanical attachment and the thermal link through which the heat must flow as it moves from the absorber to the detector body. The joint may perform a thermalizing role as well, but the importance of this function has not been established by experiment.

We will now discuss the design of the different elements of the detectors -- the thermometers, the thermal link/mechanical support, and the absorber. We will review the performance of these detectors, and discuss the ultimate performance expected from optimized detectors using this technology.

3.1 Thermometers

We use heavily doped Si as the thermometric element in our detectors. These thermometers are made by ion implantation into the Si body of the detector, a process which fits naturally into the fabrication process for our monolithic arrays of microcalorimeters. The conduction mechanism in this heavily doped silicon is phonon assisted hopping; the resistance of such detectors rises rapidly with decreasing temperature. This type of thermometer has been widely used for infrared bolometers and cryogenic thermometry.

Since the thermometer element dominates the heat capacity in many of our detectors, its optimization should result in overall performance improvement. Initially, (Ref. 2) we had assumed that the thermometer heat capacity could be minimized by reducing its volume. Early experiments showed that two factors degrade the performance of small thermometers. The optimal bias power for an ideal microcalorimeter depends linearly on its thermal conductance. With fixed thermometer volume, the optimum power density in the element increases as the thermal conductance rises. At some power density level, the thermometers begin to lose thermal sensitivity. Further increases in bias power up to the ideal "optimal" level actually result in a decline in performance. For a given value of thermal conductance, there exists an optimal thermometer volume. A smaller element would have reduced sensitivity due to excessive bias power density. A detector with a larger element would have lower performance due to the additional heat capacity.

The thermometers also have significant current noise. This effect scales as $V^{-0.5}$, where V is the thermometer volume. This variation indicates that the noise arises in the thermometer, rather than its contacts. More careful studies of the noise scaling with thermometer resistivity are required for defining its role in an optimal thermometer.

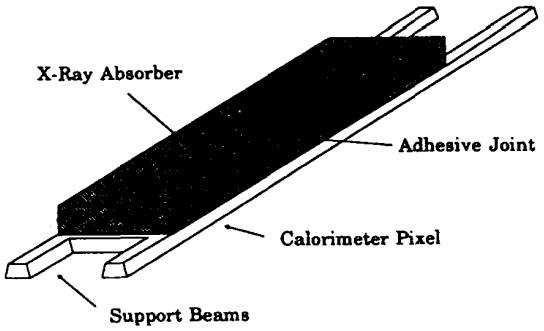

Figure 4. Schematic of a monolithic detector with an epoxy attached absorber. The detector is connected to its heat sink through the four trapezoidal links. They are each typically 2.5 mm long, and are ~10 μm across the top surface, 8 μm thick, and the sides make a 55 degree angle with the top surface. The thermometer is implanted into the detector body, and the ion implanted electrical connections are implanted into the thermal links. The absorber is attached to the detector body with a small epoxy joint.

Another parameter which can be varied in the optimization is the resistivity of the thermometer element. We constrain the thermometer to have a resistance in the range from 10^7 to 5×10^7 Ω for best noise performance with existing JFET amplifiers by changing the aspect ratio of the resistor. Variation of

the impurity concentration changes the resistivity and the temperature coefficient of resistance of the thermometer. As we decrease the impurity concentration, the resistivity of the thermometer increases, and its temperature coefficient α increases. The higher temperature coefficient does not come without a cost. The higher resistivity thermometers begin to be affected by reduced sensitivity and excess noise at a lower power level than less sensitive, lower resistivity thermometers. Therefore, we cannot achieve the full benefit expected by using the higher sensitivity thermometer. A detailed study is underway to obtain the information to allow us to carry out an optimization of the thermometer allowing for its non-ideal behaviors (Ref. 6).

Several concepts for improved thermometers have been proposed. Some of the most interesting are nondissipative devices which in principle have no thermal noise. Two such devices are the kinetic inductance thermometer (Ref. 7), and the capacitance thermometer (e.g. Ref. 8). In the kinetic inductance thermometer, the temperature is measured as a change in the inductance of a superconducting stripline. The dependence of inductance on temperature is weak when operating significantly below the superconducting transition, but since we are using a superconducting sensor, we can read it out with sensitive SQUID amplifiers. Used in this way, these thermometers look very appealing. The capacitive thermometer is conceptually similar, in that the temperature is determined by a change in the capacitance of a sensor. Again, the temperature coefficient is small, but very large voltage biases can be applied. (Note that in both thermometers, during readout the sensors have high energy densities. They must be nearly dissipationless in order to function at all.) Both devices are interesting, but their low noise performance has not been experimentally verified. Again, to realize the benefits of improved thermometers, the heat from the absorbed X-ray must arrive promptly at the thermometer; that is, the thermal signal itself must have large bandwidth.

3.2 Thermal Link and Mechanical Support

In the monolithic detectors, the mechanical support serves the function of providing the thermal coupling to the heat sink. The value of the conductance of the thermal link does not affect the resolution of an ideal microcalorimeter (Ref. 2). As the thermal conductance is increased, the required bias power for optimal sensitivity with a resistive thermometer increases proportionally, and the detector time constant becomes proportionally shorter. However, the sensitivity of the Si impurity thermometer is reduced when operated with high bias power density, so high thermal conductances result in lower sensitivity. Also, given the imperfect thermal connection between the absorber and the detector body, the speed of a practical detector is limited. These practical considerations require that the thermal conductance be less than a certain value depending on the thermistor size and the overall heat capacity.

The mechanical supports are thin Si beams, produced by anisotropic etching of the single crystal Si. In Si at low temperatures, the phonon mean free path is significantly longer than the transverse dimensions of the legs. Therefore, the conductance of these supports is dependent on exactly how the phonons interact with the surfaces of the support legs. For smoothly etched surfaces, we have measured conductances which imply that almost no scattering occurs at the leg surfaces. In this case, the thermal conductances of the supports are higher than desired. Since these supports are already as small as is practical to produce using our current process, we have sought to reduce the conductance by reducing the phonon mean free path by increasing the scattering at surfaces. We have developed a technique for producing a rough rear surface on the support leg. The wet-etch process produces a distribution of pyramids on the rear surface, with scale sizes ranging from 5 μm down to less than 1 μm. The scattering efficiency of this surface is apparently high, because the thermal conductance of detectors with this texturing is substantially lower than that of those with smooth surfaces. With the surfaces textured as described, the conductance of the detector legs described in Fig. 4 is approximately

$$G(T) = 2.0 \times 10^{-11} (T / 0.1K)^3 \, W / K. \qquad (5)$$

This conductance is remarkably constant among the devices of this design we have evaluated.

For detectors with the thick absorbers of relatively high heat capacity, suitable for use on the AXAF XRS instrument, the thermal conductance we have achieved is very close to the optimal value. If we wish to produce detectors optimized for operation at lower energies (e.g. for the 100 eV to 1 keV range) where the heat capacity of the absorber is much smaller, better performance could be achieved using lower thermal conductance detectors. Work is in progress to make supports with more than an order of magnitude smaller cross sectional area which can support the detectors, but which should have much lower thermal conductance.

3.3 Absorbers

The study of candidate absorber materials has been a major element of our program over the past several years. Without an efficient and low noise thermalizer, high resolution spectroscopy is impossible. Some of our very early results showed excellent thermal sensitivity, that is, each X-ray photon was detected with a high signal to noise ratio, but there was substantial variation in the pulse height from one event to another (Fig. 3). In this spectrum, the baseline at zero energy is generated by sampling the detection filter randomly in the absence of X-rays. The width of this baseline is due to the detector noise and any amplifier noise. The X-ray lines are broader, because they are influenced by all the factors contributing to the width of the baseline, plus the variation in the fraction of energy thermalized from event to event. The quadratic difference in the width of an X-ray line and the baseline shows the variation in thermalized energy, which we call thermalization noise. In this case, the X-rays were being absorbed in high resistivity (100 Ωcm) Si. It was inferred that the variation in energy detected is due to variations in the amount of energy stored as trapped charge.

We tested a variety of available absorber materials in our laboratory, including HgCdTe. The idea here was to try an absorber with smaller bandgap energy in

order to reduce the energy loss associated with trapping. HgCdTe has a bandgap that depends on the relative concentration of Cd. This material had been grown by Rockwell International to have a 0.060 eV bandgap at 77 K (10% Cd); the gap is somewhat smaller at lower temperatures. Tests carried out with this material showed low heat capacity, and quite good thermalization. The residual thermalization noise was about 11 eV at 6 keV; a good detector was required to detect this broadening (Ref. 9).

To go below the 11 eV broadening of the HgCdTe, we chose its close relative, the zero-gap semimetal HgTe. Using this material, we were able to obtain excellent spectral resolution (Fig. 5). This material proved to be an excellent thermalizer, with any excess broadening due to metastable energy storage $\leq$ 3 eV FWHM. The primary limitation of the HgTe is that the material has a relatively high ratio of heat capacity to X-ray absorption. Significant improvements require that we find a material which has a substantially lower heat capacity than the HgTe, but has good X-ray absorptivity and thermalization properties.

A class of absorbing materials which has the promise of low heat capacity and good thermalization efficiency is superconductors. If used at temperatures far below their superconducting transitions, the heat capacities of these materials are their Debye heat capacities; all the electrons are frozen in the superconducting ground state and do not contribute significantly to the system heat capacity. When an X-ray interacts with a superconductor, much of the energy of the event goes into the breaking of Cooper pairs into quasiparticles. Energetic quasiparticles can lose energy through inelastic scattering, but quasiparticles at the gap energy must recombine into Cooper pairs in order to return to the ground state energy. Far below the superconducting transition temperature there are few equilibrium quasiparticles, and recombination can be slow. Providing quasiparticle traps (Ref. 10), regions of reduced gap, can enhance the recombination rate. In principle, the superconductors are the ideal absorbers; by design we can trade heat capacity for recombination rate by increasing the equilibrium free electron density. Our experiments and those of other groups (Refs. 11,12,13) have shown that the problem may be more complicated than anticipated. Some refractory superconductors, such as Re, have very low Debye heat capacities, and therefore are excellent candidates for calorimeter absorbers. Measurements of high quality Re and Ta foils (Refs. 13,14) showed their X-ray response to be smaller and slower than expected. This could be due to a much larger heat capacity or a longer quasiparticle recombination time than expected. The large heat capacity is more likely, since the application of normal metal quasiparticle traps on the foils (Refs. 13,14),

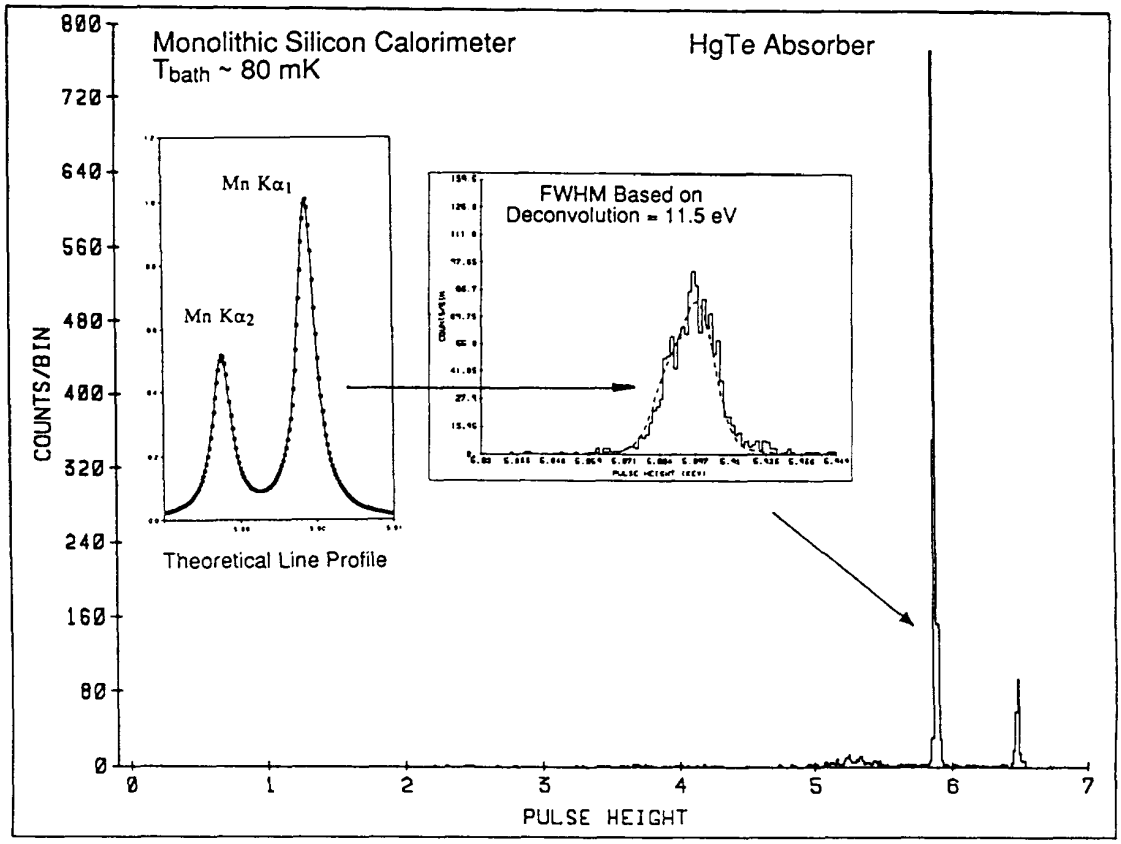

Figure 5. The spectrum of ^{55}Mn X-rays measured with a detector using HgTe. The absorber is 1 mm x 0.25 mm x 12 μm thick, and is configured as shown in Fig. 4. The resolution was determined by convolving the line profile (inset) with a Gaussian until a good fit was obtained. The derived energy resolution is 11.5 eV (FWHM), consistent with the baseline noise as determined by sampling the signal in the absence of X-rays. Any contribution to the measured width due to thermalization noise or position dependence must be less than 4 eV at 6 keV.

which should have resulted in short quasiparticle lifetimes, had little effect on the response time. The pules shape, with extremely rapid initial recovery preceding the long flat tail, cannot be explained by heat capacity alone, however.

The most successful superconducting absorber tested has been Sn (in foil form). The heat capacity of the 0.99999 pure Sn foil is near the Debye heat capacity. The response to the absorption of the X-ray has multiple time constants, with a prompt response corresponding approximately to the Debye heat capacity of the Sn, with a significant amount of the signal power in a long tail on the pulse, with time constants several times that of the initial response. At least some of this long tail may be due to the epoxy joint attaching the Sn to the Si detector body. Further experiments are required to separate the contribution of the Sn from the epoxy on the detector. The thermalization of the X-ray in the Sn is efficient; the spectral resolution is limited by the detector noise. The contribution of the thermalization noise to the line width is ≤ 3 eV FWHM at 6 keV for the Sn absorber. For the AXAF XRS experiment, we require 67% efficiency at 10 keV, which requires a 12.5 μm thick layer of Sn. With such an absorber on a 1 mm x 0.25 mm detector, we have achieved a resolution of 10 eV FWHM (Fig. 6).

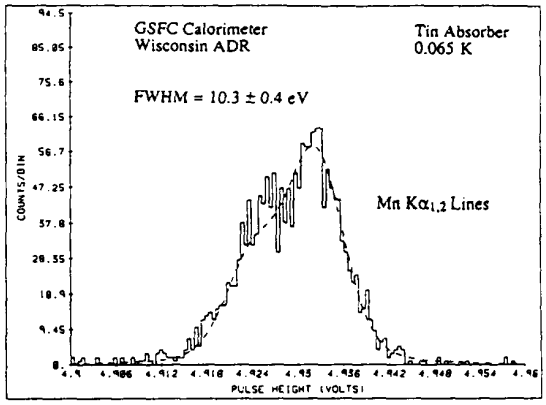

Figure 6. The spectrum of ^{55}Mn K$\alpha_{1,2}$ lines measured with a detector with a 0.6 mm x 0.25 mm x 25 μm superconducting Sn absorber. The resolution of the detector is 10 eV FWHM, again consistent with detector noise and no thermalization noise.

While the thermalization of the X-rays is efficient in the Sn absorbers, significant improvements in performance require lower heat capacity absorbers which convert X-rays to heat efficiently and noiselessly. Since the epoxy attachment of the absorber to the detector body may also have a significant effect on the detector response time, new attachments should be studied as well. The requirements for this joint may be complicated by the fact it may play a significant role in the thermalization of the deposited energy.

Current work is focused on deposition of the absorber directly on the detector, or onto a Si film which can be attached to the detector. Experiments with deposited films of Ta, Nb, and Sn have shown that there are significant variations in the performance of nominally very similar deposited films of superconductors. Apparently, some significant parameter which affects the thermalization of X-rays in these films is not being controlled in their production or test.

3.4 Amplifiers and Signal Processing

In order to achieve the sensitivity anticipated from the microcalorimeters, amplifiers with low noise in the signal bandwidth of the detectors must be used. We are free in the design of our detector to choose its operating resistance to best match the characteristics of our amplifiers. The JFET is an excellent choice for the front-end amplifier for the microcalorimeter. When operated at T ~ 77K, such a device has a noise temperatures of ~10 mK. That is, its total noise would be equal to the Johnson noise of a properly matched input resistor cooled to 0.010 K. Therefore, a properly selected JFET when operated with a microcalorimeter of the proper resistance (~5 x 10^7 Ω) should not increase the system noise significantly. In order to avoid electrical noise from instrumental vibrations (microphonics) it is desirable to mount the first stage amplifier as close to the detector as possible. This presents a challenge, since the detector is operating at T< 0.1K while the JFET amplifier typically operates at T> 70K. In the design of focal planes with large numbers of detectors, this thermal interface poses one of the largest practical problems. In current designs, the JFET's are supported on a Kevlar fiber suspension; electrical connections are made using 25 μm diameter Manganin wire. The JFET's are heated by their operating drain current. Such a system with 32 channels and 12 mW total power dissipation has been designed for the AXAF XRS experiment. (Only ~0.4 mW flows directly to the helium; the rest is dumped to the vented gas.) The amplifiers are operated as source followers, which provide a voltage gain near unity, but reduce the impedance of the signal line from ~5 x 10^7 Ω to ~2 x 10^3 Ω, reducing proportionally the sensitivity of the signal to microphonic pickup.

The signal is further amplified by a conventional low noise amplifier, and then is digitized. The digitized signal is then optimally filtered to produce the pulse height for the event (Ref. 9). The digital optimal filtering approach has played a significant role in the success of our development program. The optimal filter permits one to get remarkably good results even in the presence of significant microphonic noise or electronic pickup. In applying the optimal filter to the determination of pulse heights one must sample the signal more rapidly than one might naively guess. Since the X-rays arrive at random phase with respect to the sampling clock, we must sample rapidly enough that the variation of the derived pulse height with arrival phase is significantly less than the detector resolution.

4. SUMMARY

The performance of microcalorimeters as X-ray spectrometers is approaching initial expectations. The development of monolithic detectors with semiconductor thermometers and efficient X-ray absorbers of low heat capacity has resulted in devices

with high spectral resolution, adequate area, and with somewhat long, but acceptable response times. For applications where the photon rate is low, and we wish to extract the maximum information from each photon, the microcalorimeter is the detector of choice.

Two major factors have been important in achieving high spectral resolving power in these detectors. They are the recognition of energy trapping in some absorbers along with the selection of efficient thermalizers as absorbers, and the use of digital optimal filtering. The optimal filtering was important not so much for the few percent improvement one expects to achieve over the best analog filter under optimal conditions, but for allowing useful experiments to be done in the presence of significant electrical and microphonic interference.

Rocket and space borne experiments using microcalorimeters are under development at Goddard Space Flight Center and the University of Wisconsin, and we expect the first astronomical results in the near future.

5. ACKNOWLEDGMENTS

We would like to acknowledge the contributions of R. Brekosky, R. McClanahan, B. Mott, P. Murdock, and C. Sappington of the Goddard Solid State Device Development Branch in the production and testing of the calorimeters.

6. REFERENCES

1. McCammon, D., and Sanders, W. T., 1990, *Ann. Rev. Astron. Astrophys.*, **28**, 657.

2. Moseley, S. H., Mather, J. C., and McCammon, D., 1984, *J. Appl. Phys.*, **56**, 1257.

3. Moseley, S. H., Kelley, R. L., Mather, J. C., Mushotzky, R. F., Szymkowiak, A. E., and McCammon, D., 1985, *IEEE Transactions on Nuclear Science*, **NS-32**, 134.

4. McCammon, D., Juda, M., Zhang, J., Holt, S. S., Kelley, R. L., Moseley, S. H., and Szymkowiak, A. E., 1987, *Japanese Journal of Applied Physics*, **26**, Supplement 26-3, 2084.

5. McCammon, D. , Moseley, S. H., Mather, J. C., and Mushotzky, R. F., 1984, *J. Appl. Phys.*, **56**, 1263.

6. Zhang, J., Ph.D. thesis, University of Wisconsin, in preparation.

7. McDonald, D. G., 1987, *Appl. Phys. Lett.* **50**, 775.

8. Pfaffman, T. E., Silver, E., and Labov , S., 1990, *Proc. SPIE*, **1344**, 302.

9. Moseley, S. H., Kelley, R. L., Schoelkopf, R. J., Szymkowiak, A. E., McCammon, D., and Zhang, J., 1988, *IEEE Transactions on Nuclear Science*, **35**, 59.

10. Booth, N. E., 1987, *Appl. Phys. Lett.*, **50**, 293.

11. Labov, S., Silver, E., Pfafman, T., and Wai, Y., 1990, *Proc. SPIE*, **1344**, 295.

12. Gallinaro, G., Gatti, F., and Vitale, S., 1991, *Europys. Lett.*, **14**, 225.

13. Stahle, C. K., 1991, *The Development of High Resolution Calorimetric X-ray Detectors for Compton Scattering Experiments*, Ph.D. thesis, Stanford University.

14. Stahle, C. K. Osheroff, D., Kelley, R .L, Moseley, S. H., and Szymkowiak, A. E., 1992, *Nuclear Instruments and Methods in Physics Research*, **A319**, 393.

Development of Microcalorimeters for High Resolution X-Ray Spectroscopy

R. L. Kelley, S. H. Moseley, C. K. Stahle†, A. E. Szymkowiak, M. Juda*, D. McCammon* and J. Zhang*

NASA/Goddard Space Flight Center, Greenbelt, MD, 20771, USA
**Physics Department, University of Wisconsin, Madison, WI, 53706 USA*
†NAS/NRC Research Associate at NASA/Goddard Space Flight Center

We have been developing microcalorimeters for use in X-ray spectroscopy. These devices have very high spectral resolution (several eV) and high intrinsic quantum efficiency, making them particularly useful for astrophysical applications. Work has evolved over a 10 year period from simple proof-of-concept devices to functional arrays. An energy resolution of 7.3 eV at 6 keV has been demonstrated for the smallest absorbers used, and a resolution of ~ 12 eV for devices with a pixel area of ~ 1/4 mm^2. Present work is focused on making 36 pixel monolithic arrays with individual pixel areas of up to ~ 1 mm^2. As the size of the absorbing area is increased, high spectral resolution is more difficult to achieve not only because of the increased heat capacity, but also because of problems with obtaining uniform thermalization. We have observed non-ideal effects in large absorbers that must be controlled and minimized before the fabrication of low noise, larger area microcalorimeters can be accomplished.

1. INTRODUCTION

The development of microcalorimeters has been motivated by the need for a high resolution X-ray spectrometer that has high intrinsic quantum efficiency for use in X-ray astronomy. This is due to the very low X-ray fluxes characteristic of most celestial X-ray sources. The basic principle of the microcalorimeter is straightforward. X-rays are thermalized in a small mass at cryogenic temperatures and produce a temperature rise proportional to the photon energy that is sensed by an appropriate thermometer.[1] The theoretical energy resolution can be as low as ~ 1 eV. From the start it was realized that there may be several obstacles to achieving the theoretical resolution. The most important of these has been achieving rapid and complete thermalization of X-ray energy, and significant progress has been made thus far in solving these problems.

We have fabricated numerous calorimeter arrays and tested these with a variety of absorbers. The arrays can be classified into those with small pixels (1/4 mm^2) and those with large pixels (1.0 mm^2). On the small pixel arrays, we have used thermometers with a range of sizes from those that occupy a small fraction of the pixel area to those that cover nearly the full area of the pixel. The absorbers have consisted of small pieces of

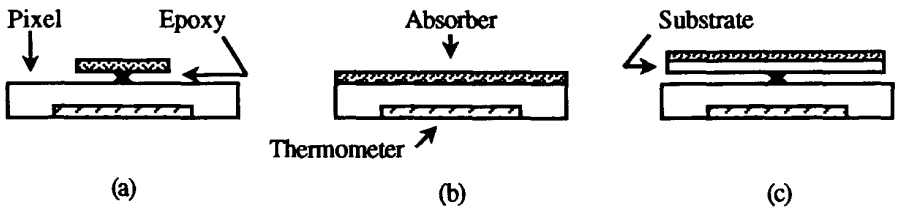

Fig. 1 Absorber attachment schemes. (a) Absorber attached directly to pixel with epoxy. (b) Absorber deposited directly onto pixel. (c) Absorber deposited onto substrate that is attached to pixel with epoxy.

bulk material and deposited films, both directly applied to the pixels and onto substrates that are attached to pixels with epoxy (Figure 1). Measurements of the X-ray response of these detectors and absorbers has provided a large amount of data that we are now attempting to use to improve the performance of microcalorimeter arrays.

2. CALORIMETER ARRAYS

The design and fabrication of calorimeter arrays has been motivated by the requirements for use in the Advanced X-Ray Astrophysics Facility (AXAF) focal plane and, more recently, for use on a sub-orbital experiment being constructed to measure the spectrum of the soft X-ray background. The small array (for AXAF) has pixels that are 0.25×1 mm and the large array (for the diffuse background experiment) has pixels that are 0.5×2 mm. The thermometers are formed by ion-implanting P compensated (typically 50%) with B into Si, and sense temperature through phonon-assisted hopping conduction. We have also fabricated test arrays that have a variety of pixel and thermometer geometries to measure the dependence of responsivity and noise on thermometer size and conductance of the thermal link.

The choice of thermometer volume is determined by a trade-off between heat capacity and thermometer sensitivity. Small thermometers have lower intrinsic heat capacity, but have a larger non-thermal term that diminishes the resistance and the temperature coefficient of resistance as the thermistor volume is decreased for fixed bias power and temperature.[2] Large thermometers degrade resolution through their high heat capacity. The optimal bias power density can be reduced by choosing a smaller thermal conductance, but then a smaller total heat capacity is required to keep the thermal time constant from increasing. We have found empirically that a thermistor size *roughly* equal to $200 \times 200 \times 0.5$ μm is close to optimum with respect to these two effects. A more careful optimization should include the effects of excess current noise that is known to scale inversely with the $\sqrt{}$(volume) of the thermometer.[3] Another factor to consider is the possible loss of non-thermal phonons (to the thermal link) before being down-converted and sensed as a single temperature phonon distribution. It may be possible to minimize this effect by making the thermometer area comparable to the pixel area. Once the required volume has been established, the thermometer geometry is determined by selecting the operating resistance and using the thermometer resistivity to determine the aspect ratio of the thermistor.

The amount of ohmic contact material used on the pixel is also potentially important. Presently, we use degenerately doped P, which should have a heat capacity that is less than 5% of the total detector heat capacity. However, a significant electronic heat capacity could result if the implanted ohmic trace diffuses into a larger volume. If so, it may be possible to eliminate this problem by using superconducting Al traces.[1]

3. X-RAY ABSORBERS

The ideal absorber has a low heat capacity and completely thermalizes photons much faster than the thermal time constant of the detector. We have generally found that materials with zero or no bandgap are best because charge trapping has less effect in these materials. However, the material should also have low lattice and/or electronic heat capacity. Among those that we have tested are InSb, Bi, HgCdTe, HgTe, and sapphire (despite the large bandgap).

Superconductors offer the potential for low heat capacity and good thermalization, since the electronic term is frozen out below T_c, and since there are no states to trap energy. Moreover, there are several superconductors that have high Debye temperatures, hence lower heat capacities. However, well below T_c quasiparticle states can be extremely long-lived compared to the thermal time constant of the detector, thus causing problems in measuring the total pulse energy. It has been found, however, that bulk Sn works reasonably well.[4] However, Sn has a Debye temperature of only 200 K, thus limiting its use to small or thin absorbers (for use at low energies). We have also tested Nb, Ta, and Re,[5] but have found these materials to give rise to long pulse decay times, indicating long quasiparticle lifetimes or high heat capacity. Gatti et al. have found similar results with Re.[6]

A fundamental issue affecting the choice of absorber is the thermalization performance of a deposited film compared with a bulk sample of the same material. This is an important concern, since it is difficult to fabricate large element arrays if the absorber must be manually attached to each pixel. We have found that there can be very large differences in the performance of the absorber depending on its morphology, and also depending on whether its is on a substrate or free-standing.

3.1 Bulk Absorbers

First, we consider small bulk absorbers. We have tested small samples of HgTe, Bi, and Sn that were attached with epoxy (typically filled Stycast or Epo-tek H74) to calorimeter pixels. A summary of the high spectral resolution results achieved with these absorbers using 6 keV X-rays from ^{55}Fe is shown in Table 1. The differences in energy resolution have more to do with the responsivity of the individual detectors used, and less with the performance of the absorbers. The 7.3 eV result with HgTe was obtained on a small pixel with a thermometer that covers about 80% the full pixel area, while the 9.4 eV result with Bi was obtained using a large pixel that has a thermometer that covers about 8% of the pixel area. The size of the absorber in each case was much smaller than the pixel.

For larger absorbers, we have tested HgCdTe, HgTe, sapphire, and Sn. We have obtained an energy resolution of 11.5 eV for HgTe with an area of 1/4 mm^2, which is the size planned for use in the AXAF focal plane array. We have also tested a relatively

Table 1 - Summary of High Spectral Resolution Results

	Absorber Size	Energy Resolution (FWHM @ 6 keV)
Bulk Absorbers:		
HgTe	< 10 μgm	7.3
HgTe	0.25 × 1 mm × 12 μm	11.5
Bi	~ 7 μgm	9.4
Sn	0.25 × 0.6 mm × 25 μm	10.3
Sn	~ 1 × 1 mm × 13 μm	21.4
Deposited Absorbers:		
HgTe (on Si)	0.25 × 0.8 mm × 0.7 μm	14.3
Sn (on Si)	0.25 × 0.5 mm × 2 μm	13.6

large sample of Sn (~ 1 mm^2 and a thickness of 13 μm) on a 0.5 × 0.5 mm pixel that has a thermometer area of about 60% of the pixel area. In this case the energy resolution was 21.4 eV and there was ~ 7 eV of excess broadening relative to the baseline noise of 20.2 eV.

Sapphire was tested in several volumes up to 1 mm^2 × 27 μm for X-ray thermalization performance in order to compare it with Si. Surprisingly, it was found that sapphire can yield an energy resolution that is two or three times better than the Si we typically use for arrays.

3.2 Deposited Absorbers

The goal with any deposited material is to obtain a film that has the same heat capacity and thermalization performance as the bulk form of the material. We have deposited the absorber directly onto the pixel (the side opposite that of the thermistor) and also deposited the absorber onto a Si substrate that is then attached to the pixel with epoxy (see Figure 1). Results from the latter approach will be discussed first. We have worked with CVD HgTe and vapor deposited Bi and Sn. For HgTe, we have found that the lattice heat capacity may be higher in polycrystalline form than single crystal HgTe, whereas for Bi and Sn films we find that it is possible to achieve heat capacities that are consistent with the bulk element values. Results for HgTe and Sn are shown in Table 1. With HgTe and Sn, we find that it is possible to obtain good energy resolution with no excess broadening for absorber areas up to about 1/4 mm^2. Thicker films of HgTe have not been adequately tested yet. With deposited Bi, we generally find that there is excess broadening of the X-ray lines with respect to the baseline. The line profiles are often non-Gaussian, with tails or smaller peaks on both sides of the X-ray line. The Bi depositions have generally not been carried out to the same standards as the HgTe and Sn depositions, and it is possible that impurities or an oxide is causing less than full thermalization in the Bi films.

We have also experimented with calorimeters where an absorber is deposited directly onto the pixel. This was done on arrays that had two independent thermometers so that a search for position dependence could be made. For two experiments the data show a clear inverse relationship between the pulse signals in the two thermometers, indicating a strong dependence on where the X-rays are absorbed.[4] This suggests that the

X-rays are not thermalizing rapidly in the film, and non-thermal phonons are propagating into the Si pixel where they are sensed non-uniformly by the (hopping conduction) thermometer depending on the original location of the X-ray relative to the thermometer. In addition, the Sn films have an X-ray thermalization function with a time scale of nearly 10 msec, which can be made much shorter by the application of a magnetic field that also improves the thermalization efficiency.[4] This suggests long quasiparticle lifetimes in the films that are not typically observed in the bulk Sn absorbers. This may be due to defects or residual magnetic impurities in the bulk Sn that enhance quasiparticle recombination. In either case, the X-rays are not being thermalized rapidly compared to the thermal time constant of the detector, as required for good energy resolution.

Thus, we find that when the absorber is deposited onto a Si substrate and then adhesively attached to the pixel over a small area compared to the pixel, the results are improved compared to deposition directly onto the Si pixel. However, even with the composite absorber scheme, less favorable results begin to appear as the absorber is made much larger than ~ 1/4 mm^2. With the same Sn deposition that gave the 13.6 eV results in Table 1, but with an area of 0.5 × 2 mm (i.e., a factor of 8 increase in area), we find that there is significant excess broadening of the X-ray lines. Moreover, if the same absorber is then apertured down to an area equivalent to the size of the smaller Sn absorber that had the 13.6 eV resolution, we find that there is only somewhat less excess broadening. Since the thermal energy is being forced into the pixel at a fixed point, this indicates the large absorber is not properly thermalizing the X-rays. One possibility is that the absorber has a low lateral thermal conductance that causes a position dependent delay of the heat flowing into the pixel, which would be sensed as a pulse height variation. Another possibility is that the Si substrate for the absorber may affect the thermalization in this case, for example due to the existence of metastable states.[1]

Experiments are under way to study this further. Recently, we compared Bi with a thickness of 2 μm deposited on ~ 10 μm Si substrates with Bi films from the same deposition that was deposited on photoresist and then removed to produce a free-standing 2 μm Bi film. It was found that although the Bi deposition was intrinsically poor (large excess broadening even in small samples), the Bi on Si thermalizes much better than the free-standing Bi film. There is an anti-correlation between pulse rise time and pulse height for the Bi film that is not observed for the Bi on Si. This suggests that the thermal conductance of the deposited film (at ~ 70 mK) may be quite low compared to the bulk sample value. Tests will be done with Ag epoxy to make absolute thermalization measurements on the attached films.[4]

4. CONCLUSIONS

We have fabricated microcalorimeters that have high X-ray energy resolution using different absorbers and absorber attachment schemes. Improvements in resolution will almost certainly be made as the thermometers are fully optimized for minimum heat capacity and current noise, and maximum responsivity. For bulk absorbers with an area of ~ 1/4 mm^2 and thickness less than about 12 μm (the size to be used for the AXAF focal plane array) we find that an energy resolution of < 12 eV is readily achievable using HgTe or Sn. An energy resolution of ~ 21 eV has been achieved with a large (~ 1 mm^2) Sn absorber.

For absorbers that are deposited directly onto the calorimeter pixels, non ideal effects are observed that limit the energy resolution. Improvements in this approach may be achieved by obtaining films that thermalize X-rays much faster than the thermal time constant of the detector and optimizing the geometry of the thermometer to minimize the effects of non-thermal phonons.

Progress is being made with absorbers deposited on substrates that are then adhesively attached to the pixel. The use of an absorber substrate with a small attachment point significantly improves thermalization compared with depositing the absorber directly onto the pixel. For thin (< 2 μm) absorbers, we find good thermalization performance and energy resolution with HgTe and Sn for sizes up to about ~ 1/4 mm^2. As the area of the absorber approaches ~ 1 mm^2, there are effects that limit the energy resolution that are being investigated. These may include variations in the thermalization function in thin films due to low thermal conductance and metastable states in the film and/or absorber substrate.

For superconducting absorbers, the goal is to decrease the thermalization time. This can be done with the application of magnetic field to trap flux, and thus enhance quasiparticle recombination. Alternatively, it may be possible to use a superconductor with a T_c that is closer to the operating temperature of the calorimeter, which will yield higher quasiparticle densities, and thus higher recombination, but perhaps at the expense of increased heat capacity. This would require a trade-off between enhanced thermalization performance and additional heat capacity.

The problems we are addressing in large deposited films are likely to be present at a lower threshold in smaller deposited absorbers. Thus, as we attempt to improve the performance of the large films, the ultimate energy resolution of small calorimeters should also improve. However, the use of bulk absorbers with areas of ~ 1/4 mm^2 offer high spectral resolution throughout the 0.1 - 10 keV that can be used for astrophysics now.

ACKNOWLEDGMENTS

The authors are grateful to members of the Electronic Device Development Section at Goddard. In particular R. Brekosky, R. McClanahan, B. Mott, P. Murdock, and C. Sappington. We also thank J. Dubowski, M. Gaidis and S. Wu for the HgTe, Sn and Bi films. C. K. Stahle acknowledges an NRC - NASA Research Associateship.

REFERENCES

1. S. H. Moseley, J. C. Mather and D. McCammon, J. Appl. Phys. 56, 1257 (1984)
2. J. Zhang et al., Phy. Rev. B, 48, 2312 (1993)
3. D. McCammon et al., Nucl. Instr. and Meth. A326, 157 (1993)
4. C. K. Stahle et al., these proceedings
5. C. K. Stahle, Ph. D. Thesis, Stanford University (1991)
6. F. Gatti, S. Vitale and A. Barabino, Nucl. Instr. and Meth. A315, 260, (1992). Also see these proceedings

Thermalization of X-rays in Evaporated Tin and Bismuth Films Used as the Absorbing Materials in X-ray Calorimeters

C. K. Stahle†, R. L. Kelley, S. H. Moseley, A. E. Szymkowiak, M. Juda*, D. McCammon*, J. Zhang*

NASA / Goddard Space Flight Center, Greenbelt, MD 20771, USA
** Department of Physics, University of Wisconsin, Madison, WI 53706, USA*
†NAS / NRC Resident Research Associate at NASA / Goddard Space Flight Center

We have investigated the use of evaporated tin and bismuth films as the absorbing materials in X-ray calorimeters. When the films were deposited directly on monolithic silicon calorimeters, the output signal from both Sn and Bi devices was strongly dependent on the location of the absorption event relative to the ion-implanted thermistors, presumably indicating thermistor sensitivity to a non-thermal spectrum of phonons. With Sn films we also observed that a component of the thermalization proceeded slowly, relative to a complete thermalization reference. The thermalization function could be modified by trapping magnetic flux within the film. In order to distinguish thermalization effects in the films from the thermistor sensitivity to energetic phonons, we deposited Sn and Bi films on thin Si substrates which we then affixed to calorimeters using epoxy. With glued Sn films, we were able to attain as good as 13.6 eV resolution of 6 keV X-rays with no excess broadening of the line beyond the width of the baseline, while similarly made Bi devices showed excess broadening.

PACS numbers: 82.20Rp, 78.70-g, 74.40+k

1. INTRODUCTION

A calorimetric X-ray detector comprises at least three essential components. These are an absorber to thermalize the incident photons, a thermometer to measure the resulting temperature increase, and a weak link to a cryogenic heat sink. We have developed calorimeters in which a pixel containing an ion implanted thermistor and silicon beams, which serve as the weak link, are formed from a single piece of silicon. The absorber must then be attached to the pixel. In most cases this creates a fourth component, the adhesive used for the attachment. We have achieved our best resolution this way; a device with a crystal of HgTe epoxied to the pixel produced 7.3 eV resolution of 6 keV X-rays.[1] Nevertheless, it is difficult to apply epoxy in a reproducible manner and there are tails on our signal pulses which, by comparison with pulses from bare pixels, are directly attributable to the epoxy. For these reasons, we experimented with the direct deposition

of absorber material onto calorimeter pixels. This paper discusses those experiments and others designed to separate effects due to properties of the films from those due to the good thermal contact between the absorber and pixel over the full area of the pixel.

2. CALORIMETERS AND EXPERIMENTAL APPARATUS

The silicon calorimeters in our experiments were grouped together in monolithic arrays. The pixels and their supporting silicon beams were chemically etched to a thickness of about 10 μm. The other dimensions of the pixels and beams varied between devices. Thermistors were formed within the pixels by ion-implanting phosphorus compensated with boron. Electrical connection between a thermistor and bonding pads in the silicon frame was made via traces doped degenerately with phosphorous.

Devices were mounted on the mixing chamber of a $^3He/^4He$ dilution refrigerator, which was regulated at a temperature near 50 mK for most of the experiments to be discussed. An ^{55}Fe source supplied 6 keV X-rays.

A constant bias voltage was placed across the series combination of a thermistor and a load resistor. When the resistance of the thermistor dropped in response to the heating caused by the absorption of an X-ray photon, there was a change in the voltage drop across the thermistor. This change and the subsequent recovery formed the signal pulse, which was amplified. We digitized and recorded the pulses and filtered them digitally.

3. TIN AND BISMUTH FILMS DEPOSITED DIRECTLY ON CALORIMETER PIXELS

Deposition of the Sn and Bi films was done via evaporation through a mask. M. Gaidis of Yale University deposited 4 μm of 99.999% pure Sn after having cleaned the pixel surface *in situ* using an oxygen plasma. With the assistance of S. Wu, we used the facilities of D. Drew at the University of Maryland to deposit 2 μm of 99.9999% pure Bi. That system did not permit *in situ* cleaning of the pixels. The area of each pixel was 1 mm × 0.25 mm. Two separate thermistors were contained within each pixel. Four silicon beams supported the body. Within an array, the different detectors had different beam dimensions in order to provide a range in the value of the thermal conductance. For the devices used, this value ranged from 2 to 6×10^{-11} W/K $(T/0.1)^3$.

Data acquired with the Sn devices showed a broad, non-Gaussian distribution of pulse heights for a single photon energy. The variation was contained in a spike on the pulse; the pulses decayed to the same tail on the time scale of milliseconds. Acquisition of data using both thermistors in a single pixel showed that the two pulse heights were anti-correlated. Scanning a 70 μm X-ray spot across the device demonstrated an increase in pulse height as the absorption site approached the sensing thermistor. We presume this effect to be a result of anomalous thermistor sensitivity to energetic phonons. Figure 1 shows a plot of pulse height on one thermistor versus the concurrent pulse height on the other thermistor on the same detector for exposure through a 0.5 mm aperture across the width of the pixel. Both data sets were optimally filtered. The two arcs were produced by the absorption of the Mn Kα and Kβ X-rays in the Sn. The inset shows the range of pulse shapes corresponding to the spread in pulse heights.

Thermalization of X-rays in Evaporated Tin and Bismuth Films

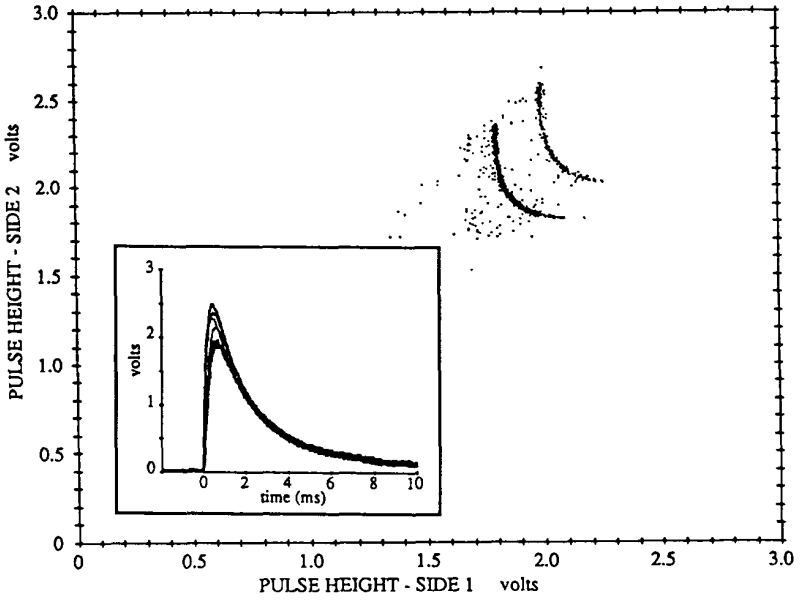

Fig. 1 Position dependence in a detector with a Sn film absorber, shown by plotting the signal obtained from a thermistor at one end of the device versus that from one at the other end. The inset shows the pulse shapes associated with the range in pulse heights.

After these initial studies, about 25000 μm^3 of Epotek H20E silver-filled epoxy was placed on the Sn side of two devices in the same array having conductances of 2 and 4×10^{-11} W/K $(T/0.1)^3$. This was done to provide a complete thermalization reference. Signal pulses resulting from the absorption of 6 keV photons in the Ag epoxy rose faster, peaked higher, and decayed to baseline more quickly than those resulting from absorption in the Sn. Data were acquired for both of these devices over a range of applied biases, biasing one thermistor while shorting the other in the same pixel. We averaged the Ag events in the Mn Kα line. To construct an average Sn pulse shape, we selected pulses from the lower end of the Sn distribution, within the Kα line, to minimize distortion by the anomalous spike. Taking the Ag pulse shape as the impulse response, we deconvolved it from the Sn pulse shape to obtain the thermalization function. The result was run through a digital low pass Bessel filter with a cutoff at 1.2 kHz. Figure 2 shows the averaged pulses and the deconvolution for the higher conductance device at the bias which maximized pulse height. The deconvolution shows an initial impulse, after which thermalization proceeds increasingly slowly, with a time constant of 6 ms characterizing the decay at 10 ms after the peak. Nearly the same thermalization function was produced at different biases for this and the lower conductance device though the decay times of the pulse pairs used in the deconvolutions varied. The slow part of the thermalization function was common to all; what differed was the magnitude of the impulse. That discrepancy could be due to incorporating varying amounts of the hot phonon spike in the average Sn pulse shapes.

The detectors were heated and allowed to cool through the Sn superconducting

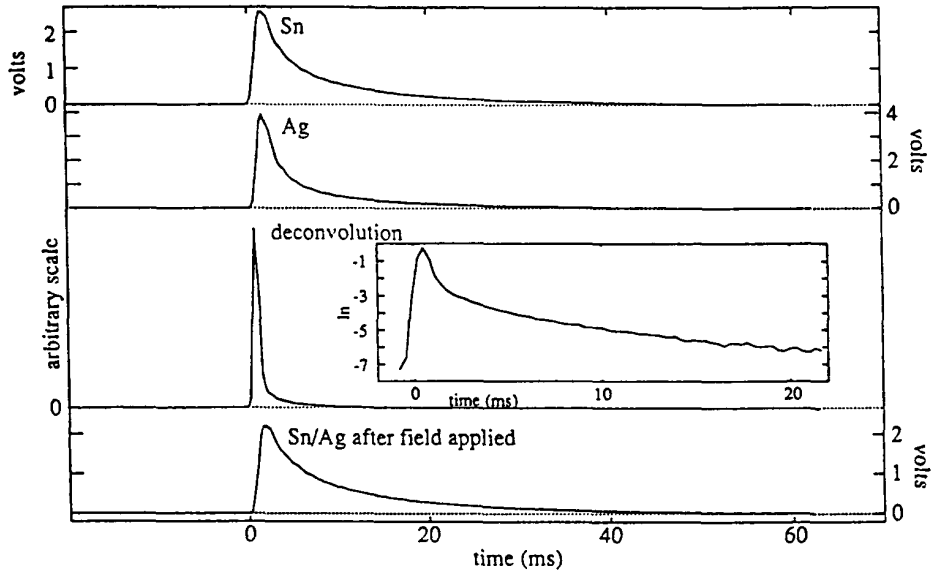

Fig. 2 Average Sn and Ag pulses and the resulting deconvolution before applying a magnetic field and the average pulse after applying a field, at which point the Sn and Ag events were no longer distinguishable.

transition in the presence of a magnetic field. The field component normal to the film was determined to be 3.2 gauss at the detector position. Upon cooling back to operating temperature, the Ag events could no longer be distinguished from the Sn events, and the new distribution was slightly displaced to lower pulse heights than the former Sn distribution. The last pulse in Figure 2 shows the pulse shape under these conditions, the average again being taken of events in the lower portion of the distribution.

The detectors were again heated and cooled in the absence of applied field. The distinct Ag population reappeared, shifted to somewhat higher pulse height, and the Sn distribution shifted to substantially lower pulse height. The Ag pulse shape was essentially unchanged from the condition prior to applying the field, but the decay time of the average Sn pulse shape was about 1.5 times longer than that of the earlier Sn pulse. This was reflected in the deconvolution, in which a time constant of 14 ms characterized the decay at 10 ms after the peak.

Since the heat from absorbing a photon in the Ag epoxy must travel through the Sn and the Sn/Si interface, the difference between the Sn and Ag pulses must result from differences in thermalization, except for thermistor sensitivity to non-thermal phonons. We attribute the slow part of the deconvolved thermalization function to the quasiparticle lifetime in the Sn during the non-equilibrium condition following X-ray absorption. The thermalization time was invariant, showing that the recombination rate is not determined by the rate of conduction of phonons away from the device nor on the operating temperature, which ranged from about 50 mK to 130 mK for the range of bias conditions. After applying a field, trapped flux apparently increased the quasiparticle density, allowing the Sn to thermalize as effectively as the Ag at the cost of increased heat capacity. Cycling through T_c without applying a field apparently left less trapped flux than present

upon initial cool-down, rendering an even longer decay time. Since this had little effect on the Ag pulse shape, this shows that large changes in the thermalization rate can be achieved without a prohibitive increase in heat capacity.

Devices with directly deposited Bi films also showed position dependence. A plot of pulse height of one thermistor versus that of the other thermistor on the same pixel displayed arcs similar to those for Sn in Figure 1. An attempt to establish a complete thermalization reference using Ag epoxy was inconclusive. Pulse shapes indicated poor thermal contact between the Ag epoxy and the film which complicated interpretation.

Because position dependence is seen with both Bi and Sn films, we conclude that this effect is not primarily a result of thermalization processes in the superconductor. We postulate that the thermistors are sensitive to the energy distribution of the phonons. Conduction in heavily doped semiconductors at low temperatures proceeds via variable range hopping.[2] The probability of an electron hopping should depend not only on the average energy density of the phonon field but on the actual energy distribution of the phonons. Superconducting absorbers may be more prone to this effect because the spectrum of phonons leaving the film is peaked at the energy of the gap. The position dependence implies that the spectrum is downgraded as the phonons propagate. The detectors also may be sensitive to the directional dependence of phonon propagation.

4. COMPARISON WITH FILMS DEPOSITED ON SEPARATE SUBSTRATES AND WITH BULK ABSORBERS

To separate effects due to properties of the films from the position sensitivity, 2 μm of Sn and Bi were deposited on 10 μm thick Si substrates using the procedures described in Section 3. Areas ranged from 2 mm × 0.5 mm to 0.25 mm × 0.5 mm. A roughly 25 μm diameter sphere of Stycast 2850 epoxy was used for the attachment to a pixel.

We have been able to obtain very good resolution with a number of attached Sn/Si absorbers, including 13.6 eV with no excess broadening beyond the width of the baseline distribution, as determined by the fit of a Gaussian to the distribution of heights resulting from random triggers in the absence of signal. When roughly 25000 μm^3 of Epotek H20E silver-filled epoxy was placed on this device, the complete thermalization reference line appeared at slightly higher pulse height than the events occurring in the Sn. A filtered deconvolution of the average Sn and Ag pulse shapes yielded only a delta function, the difference apparently obscured by the noise and by the finite time constant associated with the epoxy joint. After this device was cooled through the Sn T_c in the presence of a 30 gauss field, the Ag events could no longer be distinguished. Though the trapping of magnetic flux increased the device heat capacity, diminishing its responsivity, the resolution was good enough to see the Ag feature had the lines simply scaled with the change in heat capacity. The two populations again separated after the device had been heated and cooled through T_c in the absence of applied field. In yet another case, a resolution on 22.6 eV was obtained, compared with a baseline of 17.3 eV, but exposure to 30 gauss, without first heating the device, trapped enough flux to diminish the responsivity slightly, yet improved the resolution to 17.3 eV with no excess broadening. These results and others similar have been obtained with absorbers of area 0.25 mm × 0.5 mm which were fully illuminated. Tests with 2 mm × 0.5 mm absorbers have shown considerable excess broadening even with restricted apertures.

All of our detectors with attached Bi/Si absorbers produced broad, non-Gaussian spectral line shapes, with results from two separate evaporations being quite different. The best was a 0.25 mm × 1 mm Bi absorber with 28.5 eV resolution, ignoring a shoulder on the line shape, but the baseline noise distribution had a FWHM of 14.5 eV. We do not understand the origin of the observed thermalization noise in Bi films, though we note that the Bi depositions were not done to the same standards as the Sn depositions.

We have had success with of 99.999% pure Sn foil absorbers. We have obtained 10.6 eV resolution with no significant excess broadening with a device using a 25 μm × 0.5 mm × 0.2 mm foil. We typically see little excess broadening with Sn foils, even 13 μm ones of area several times larger than this one. Attempts to create a complete thermalization reference using Ag epoxy have not yielded significant results for Sn foils.

A roughly 7 μg piece of Bi was sliced from a piece of Bi shot from the same stock that had been used in the evaporations. When this was glued to a calorimeter, a detector was produced with a resolution of 9.4 eV for 6 keV X-rays with no excess broadening.

6. CONCLUSIONS

The direct deposition of Sn or Bi films on calorimeter pixels does not yield devices with high resolution. We have separated three effects. The first is position dependence resulting from thermistor sensitivity to the initial non-thermal spectrum of phonons. Solutions to this problem include filling the entire pixel area with thermometer (at the expense of increased heat capacity), restricting absorber and pixel contact to a small, well-defined point, and inserting a buffer layer between absorber and pixel which can thermalize phonons. The second is, in the case of Sn, delayed thermalization due to long quasiparticle lifetimes at temperatures far below T_c. This can be manipulated through increasing the equilibrium quasiparticle background through trapping magnetic flux or incorporating magnetic impurities into the superconductor. The third is a thermalization problem apparent in Bi films and large area Sn films. We have demonstrated with a bulk sample that Bi is not an intrinsically bad thermalizer. We do not yet understand the effect of geometry on thermalization, though we suspect the thermal conductance along the film and through the film-substrate interface to play a role.

ACKNOWLEDGEMENTS

We are grateful to M. Gaidis and S. Wu for the Sn and Bi depositions. C. K. Stahle acknowledges a National Research Council - NASA Research Associateship.

REFERENCES

1. D. McCammon, W. Cui, M. Juda, P. Plucinsky, J. Zhang, R. L. Kelley, S. S. Holt, G. M. Madejski, S. H. Moseley, and A. E. Szymkowiak, Proc. PANIC XII -- Nucl. Phys., A527, 821c (1991)
2. B. I. Shklovskii and A. L. Efros, Electronic Properties of Doped Semiconductors, (Springer-Verlag, Berlin, 1984)

A Silicon Composite Thermal and Ionization X-ray Detector

C. K. Stahle†, J. Wouters*, R. L. Kelley, S. H. Moseley, A. E. Szymkowiak

NASA / Goddard Space Flight Center, Greenbelt, MD 20771, USA
** Instituut voor Kern- en Stralingsfysica, K. U. L., B-3001 Leuven, Belgium*
† NAS / NRC Resident Research Associate at NASA / Goddard Space Flight Center

We have made a combination calorimetric and ionization X-ray detector by attaching a silicon p-i-n diode to a monolithic silicon microcalorimeter. Applying a bias to the diode enhanced the thermal signal, and with a reverse bias of 25 V we achieved a detection threshold of 8 eV, based upon energy scaling of the standard deviation of the baseline noise. We were able to measure a charge signal in the absence of applied bias on the diode, demonstrating that the junction potential is sufficient to drift the ionized charges to the contacts. A fraction of the electron-hole pairs created became trapped, manifested by excess broadening in the measured thermal signal and by using the variation of the thermal signal magnitude with reverse bias to fit for the fraction of charge that is trapped. The ability to collect charge without an applied bias is necessary to produce high resolution combination thermal and ionization detectors.

PACS numbers: 29.40Vj, 29.40Wk, 07.85+n

1. INTRODUCTION

Since a calorimetric X-ray detector measures the temperature increase following the absorption of a photon, the energy of the photon must be completely and rapidly converted to heat. We have developed monolithic silicon X-ray calorimeters operated at temperatures less than 0.1 K which can measure the energy of a 6 keV photon with 7 eV resolution.[1] To obtain such resolution, it has been necessary to attach an absorber such as HgTe to the calorimeter because of poor thermalization of X-rays in silicon.

When an X-ray photon is absorbed in silicon, about two thirds of the energy is quickly thermalized and the remainder goes into the production of electron-hole pairs. This can be recovered as heat when the electrons and holes recombine, but carriers can become localized in long-lived bound states before recombination can occur, causing incomplete thermalization. Since the amount of charge trapped varies from event to event, this degrades the resolution of a calorimeter with no absorbing overlayer.

We have investigated whether the application of an electric field can enhance thermalization in silicon by drifting the charges to metallic contacts where they can readily thermalize. The use of the built-in potential of a diode was of particular interest

for this application because it would do no net work on the charges. In an applied field, the work done on the charge is converted to heat in addition to the initial energy deposited by the photon. This phenomenon, which we will refer to as the Luke effect[2], enhances the thermal signal, but this does not improve resolution because the amount of charge drifted varies from event to event, and the statistics of charge production limit the resolution. At zero bias, however, if all the charge is thermalized, it is inconsequential what the initial partition between phonons and electron-hole pairs may have been since no additional energy is given to the charge. If such a scheme proved workable, an all-silicon calorimeter could, in principle, be fabricated. The measurement of the ionization signal would not be necessary, and in the interest of eliminating sources of noise and easing fabrication, the diode in such a calorimeter would be electrically shorted at the device.

The development of combination calorimetric and ionization detectors has also been proposed for dark matter detectors.[3] The difference in ionization efficiency of photon absorption and nuclear recoil for particles of the same incident energy would enable identification of the type of particle by comparison of the thermal signal and charge signal for the same event. Efficient charge collection at zero bias would permit measurement of the ionization signal with minimal degradation of the resolution of the thermal signal.

2. DESCRIPTION OF DEVICE AND MEASUREMENT APPARATUS

The diode used in our experiments was fabricated by Canberra. It consisted of a 75 μm thick, nearly intrinsic n-type region between p^+ and n^+ contacts. The n side contact filled the 2 mm × 2 mm device area, but the p side contact was a circle of 1.0 mm diameter. The body of the calorimeter selected for this experiment measured roughly 1 mm × 0.75 mm × 10 μm and was suspended within a silicon frame by four silicon beams, each about 20 μm wide and 2.3 mm long. Two thermistors were formed in the body of the calorimeter by ion implantation. Doped traces in the beams made electrical connections between each thermistor and bonding pads on the frame. The device was mounted in a half inch diameter flat pack with 25 μm diameter aluminum bonding wires bridging the bonding pads on the array and the bonding pads on the flat pack. Aluminum bonding wires were also attached to the aluminum contacts on the n and p sides of the diode, each with its far end free. A drop of Stycast 2850 epoxy, roughly a sphere of 25 μm diameter, was used to attach the diode to the calorimeter body. It was oriented with n side towards the calorimeter. The free ends of the bonding wires were connected to pads in the flatpack using Epotek H20E silver-filled conductive epoxy.

The flatpack was mounted to the mixing chamber of a $^3He/^4He$ dilution refrigerator. It was exposed to radiation from an ^{55}Fe source through an aperture. Most data were obtained with the n side towards the source. Typical base temperature of the mixing chamber was determined previously to be 47 mK. We estimate the maximum amplitude of the fluctuations experienced after settling down to the base temperature to be 0.16 mK.

The thermal signal was obtained by placing a bias across the thermistor and a load resistor and amplifying the change in the voltage drop across the thermistor as its resistance responded to the temperature change in the device following the absorption of an X-ray photon. Only one thermistor was run at a time. We used a 15 mV bias, which caused the device to operate at a temperature of 0.1 K. The charge signal was obtained by using an amplifier feedback loop to maintain the n side as a virtual ground. This placed a

ground plane between the diode and the thermistor so field dependent effects in the calorimeter could be avoided. When electrons were swept to the n side a current flowed in the feedback loop, producing a positive voltage spike as the output. This was amplified and filtered. Digitized thermal and charge pulse pairs were recorded.

3. RESULTS AND ANALYSIS

Data were accumulated for the case when the diode p side was grounded and for reverse biases from -1 V to -25 V. The device would support a forward bias of up to about 5 V without drawing current. Enhancement of the thermal signal was seen at these forward biases as well as at the reverse biases. For biases from 0 V through -3 V, there was a wide range of thermal events which were unaccompanied by a charge pulse or were paired with a charge pulse of the wrong polarity. Only those thermal pulses paired with positive charge pulses could be resolved into the Mn Kα and Kβ lines from the ^{55}Fe source, at 5.9 keV and 6.5 keV. While we cannot explain the anomalous events, they appeared to be associated with the edges of the junction. We could easily discriminate against them using the ionization signal, and their presence did not seem to affect the K lines and how their positions in the spectra varied with applied bias to the diode.

Because the applied field does work on the ionized charges, the slope of a plot of the heat generated versus bias for a particular photon energy reveals the amount of charge participating. We assume that the height of the filtered thermal pulse is proportional to the total amount of heat deposited into the device after a photon is absorbed. We do not need the absolute relationship between pulse height and energy since the information of interest can be derived from scaling the pulse heights to the response at zero bias. Writing E_{av} for the average amount of energy required to create an electron-hole pair, E_g for the band gap, n for the fraction of charge trapped, E_{trap} for the average energy a trapped pair loses to phonons prior to trapping, and e for electron charge, the ratio of heat, W, produced at a given bias, V, to that when the junction is shorted is given by

$$\frac{W(V)}{W(0)} = 1 + \frac{(1-n)eV}{\left(E_{av} - \left(E_g - E_{trap}\right)n\right)} = 1 + mV \qquad (1)$$

In silicon, for temperatures approaching 0 K, the bandgap is 1.165 eV, and one electron-hole pair is produced on the average for every 3.7 eV of X-ray energy.[4] The average energy level of the traps was not known, but for the purpose of the analysis we will assume it to be much smaller than E_g. The normalized slope of pulse height as a function of bias, m, therefore can be used to solve for n, the fraction of charge trapped, assuming that number to be independent of applied bias.

After digital filtering and correlating the thermal events with charge events of the expected polarity, the position of the 5899 eV Mn $K\alpha_1$ line was determined in each data set by the fitting of a double Gaussian to the α_1, α_2 lines in each spectrum. The FWHM in volts increased with bias as would be expected in the case when charge counting statistics dominate. The FWHM at zero bias was twice that of the baseline noise. This FWHM corresponds to a resolution of 186 eV, based on the difference

between the Kα and Kβ pulse heights. In the case of complete thermalization, the FWHM at 0 V would be no broader than the baseline; the extra width is an indication of thermalization noise associated with the statistics of trapping. The resolution obtained with -25 V bias was 198 eV. We did not expect good resolution at -25 V, where the dominant contribution to the heat is the Luke effect. We note, however, that since the baseline width in volts was independent of bias, we obtained a detection threshold of about 8 eV at a bias of -25 V, based upon energy scaling of the 1σ value of the noise.

The position of the 5899 eV Mn $K\alpha_1$ line as a function of bias is plotted in Figure 1; the error bars are ± 1σ, as determined from the fit of Gaussians to the lines. A straight line fit to the first five points is also shown. Note that the high bias points lie above this line, rather than below it, as would be expected from the non-linearity of the detector responsivity. A correction for non-linearity would exaggerate the response at those biases. Normalizing the slope from this fit by dividing by the value of the intercept provides $m = 0.2464 \pm 0.0062\ V^{-1}$. If we were to assume complete thermalization (n=0), this slope would give us $E_{av} = 4.06$ eV ± 0.10 eV. Using the canonical value of 3.7 eV for E_{av} and neglecting E_{trap}, we obtain $n = 0.126 \pm 0.031$. The errors quoted represent propagated 1σ values. These data suggest that the amount of charge thermalized is bias dependent at high biases, but for |V| < 6V, around 13% of the charge is not contributing to the production of heat. Our analysis was done under the assumption that $E_{trap} << E_g$. For shallow trapping levels less than 0.2 eV, the error associated with neglecting E_{trap} is smaller than the measurement uncertainty. In the absence of any knowledge of E_{trap}, the value of n we obtained from setting $E_g - E_{trap} = E_g$ in Equation 1 represents an upper limit on the amount of charge trapped. We obtain an extreme lower limit of 9% by assuming that the trapped charges thermalize completely prior to trapping ($E_{trap} = E_g$). For relatively small values of n, m is not very sensitive to the value of E_{trap}. A measure of the non-linearity, using a variable energy X-ray source and obtaining data points at more biases, would be required to determine whether the amount of charge trapped goes asymptotically to 0 with increasing bias or whether more charge is being produced in high fields than would be consistent with E_{av}.

The Luke effect analysis assumes that the amount of charge thermalized does not vary with bias. Our thermal data support that assumption for biases through -6 V. Assuming that all thermalized charge is collected, we would expect the magnitude of the charge pulses to be independent of bias for low biases. In order to investigate the amount of charge collected at each bias, we averaged the pulses associated with the Kα line. Figure 2 is a plot of the collected charge calculated from these average pulse shapes versus diode bias. Error bars based on propagating the noise on the charge signal, assumed to be uncorrelated, through the averaging, the integration over the pulse, and the conversion from voltage to current would be of the same size as the symbols used to mark the data points. Filters and any stray capacitance to ground within the feedback loop should affect the absolute but not the relative values of the computed charge. Figure 2 implies that the collected charge increases with the magnitude of the bias across the range of biases investigated. This is not inconsistent with the linear relationship found between thermal pulse height and bias for reverse biases through 6 V, shown in Figure 1, because the fractional variation in collected charge at low bias is within the uncertainty in n. The computed charge at 0 V is 35% less than that at 25 V, much greater than the 13% maximum trapping fraction calculated from the Luke effect analysis, supporting the possibility of excess charge production at high bias.

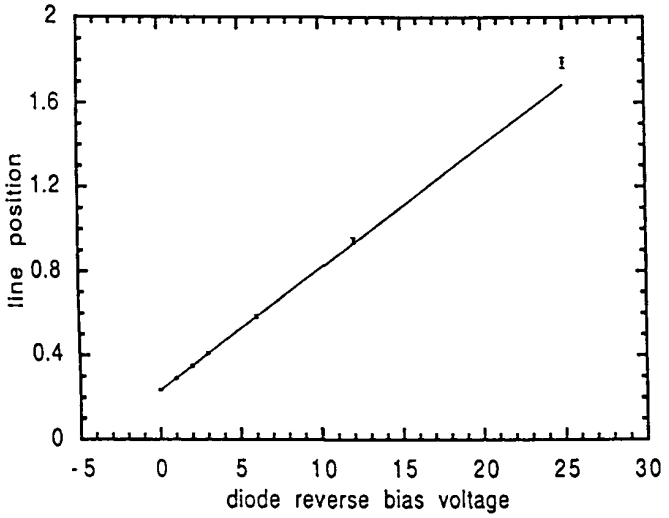

Fig. 1 Plot of position of $K\alpha_1$ line as a function of diode bias, showing a straight line fit to the five lower bias points. The error bars are $\pm 1\sigma$, as determined from the fit of Gaussians to the spectral lines.

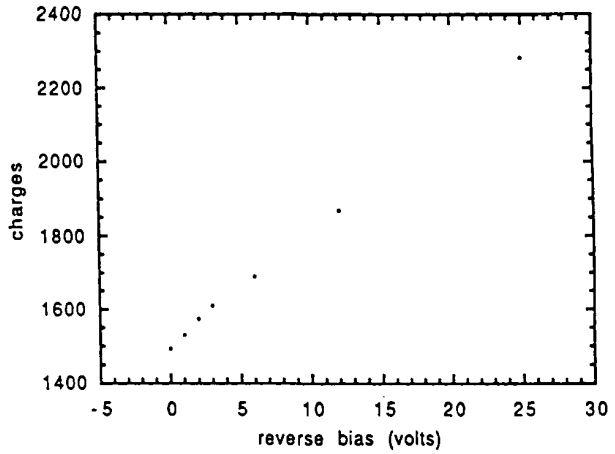

Fig. 2 Charge collected versus diode bias for charge events associated with the Kα doublet.

4. CONCLUSIONS

We have demonstrated the feasibility of running a combination calorimetric and ionization X-ray detector with the diode shorted. The junction potential alone was able to

sweep the ionized carriers to the metallic contacts, where they could thermalize, with an efficiency comparable to that demonstrated for applied biases through -6 V. Variations from event to event in the amount of charge that was not thermalized, around the average value of 13%, limited the FWHM of the 5899 eV peak to about 190 eV at zero bias. The baseline noise and device responsivity indicate that we ought to have observed a FWHM of about 90 eV in the case of complete thermalization. With -25 V bias, despite a resolution of about 200 eV, we achieved a 1σ detection threshold of 8 eV.

We expect that alterations to the diode will improve performance. We need to start with as high a purity of silicon as is practical. Shortening the drift region to the optical depth of the X-ray energy of interest may reduce trapping. We would like the intrinsic region to be fully depleted at room temperature to assure uniformity in the drift region at low temperatures. Improving the contact geometry to avoid dead regions at the corners should help to alleviate the anomalous edge effects. The active area of such a detector is constrained by the high heat capacity associated with the heavily doped contacts and should be minimized in order ultimately to achieve the best resolution, once the excess broadening is eliminated. Though 90 eV would have been the best resolution that could have been expected with the present device, that baseline was limited by responsivity (constrained by the high heat capacity and the particular thermistor properties) and by electrical noise induced by vibrations of the attached diode and its bonding wires. Although there is much work to do before a combination calorimetric and ionization X-ray detector with resolution approaching that of the best microcalorimeters is produced, this demonstration of charge collection at zero bias is a promising development.

ACKNOWLEDGEMENTS

We thank P. Burger of Canberra Belgium for the fabrication of the Si diodes and for his continued interest in this work. We thank C. Sappington of the Goddard Solid State Device Development Branch for her dedicated efforts in successfully bonding to the electrical contacts on opposite sides of the diode.

This work was done while C. K. Stahle held an NRC-NASA Research Associateship and while J. Wouters held a Fulbright fellowship providing for his visit to Goddard Space Flight Center. J. Wouters also acknowledges supplementary financial support from a NATO research grant and from the Nationaal Fonds voor Wetenschappelijk Onderzoek.

REFERENCES

1. D. McCammon, W. Cui, M. Juda, P. Plucinsky, J. Zhang, R. L. Kelley, S. S. Holt, G. M. Madejski, S. H. Moseley, and A. E. Szymkowiak, Proc. PANIC XII -- Nucl. Phys., A527, 821c (1991)
2. P. N. Luke, J. Beeman, F. S. Goulding, S. E. Labov, and E. H. Silver, Nucl. Inst. and Meth., A289, 406 (1990)
3. N. J. C. Spooner, A. Bewick, G. J. Homer, P. F. Smith, and J. D. Lewin, Phys. Lett. B, 273, 333 (1991)
4. G. Bertolini and A. Coche, eds. Semiconductor Detectors, North-Holland Publishing Company -- Amsterdam (1968)

A Prototype Kinetic Inductance Thermometer for X-Ray Calorimetry

Michael D. Audley,* Richard L. Kelley, and Gayle L. Rawley†

NASA / Goddard Spaceflight Center, Greenbelt, MD 20771, USA
**also University of Maryland, College Park, MD 20742, USA*
†Applied Research Corporation, Landover, MD 20785, USA

We have measured the parameters of a prototype kinetic inductance thermometer for X-ray calorimetry which was fabricated at GSFC. This device consists of an aluminum meander strip and ground plane and operates at about 1.2 K. For thermal isolation, the device was suspended on Kevlar threads along with a heater and a germanium resistance thermometer. The meander strip was included in the tank circuit of a 10 MHz tunnel diode oscillator operating at about 1 K. The kinetic inductance was measured by monitoring the oscillator frequency. The temperature dependence of the kinetic inductance was found to be in reasonable agreement with the behavior predicted from the device parameters. Having characterized this proof-of-concept device, we intend to investigate the suitability of kinetic inductors operating at lower temperatures for X-ray calorimetry.

1. INTRODUCTION

X-ray spectroscopy is a useful probe of the properties of astrophysical plasmas. Most cosmic X-ray sources are characterized by low X-ray fluxes and spectra which contain emission lines. Thus, high resolution and throughput are desirable for plasma diagnostics. By combining solid state detectors with conical foil mirrors moderate spectral resolution has been obtained simultaneously with a large effective area.[1] The use of X-ray microcalorimeters as detectors promises a substantial increase in energy resolution.

In X-ray microcalorimeters[2] individual photons are converted to heat and their energy is determined by measuring the resulting rise in temperature. Devices using ion implanted thermistors as the temperature sensing element have achieved a resolution of 7.3 eV at 6 keV.[3] The ultimate resolution of such devices is limited by the presence of Johnson noise. This contribution to the total noise in the device could be eliminated by using a superconducting thermometer. Infrared bolometers which use the kinetic inductance of a superconductor as the thermometric property have already been developed.[4,5]

M. D. Audley, R. L. Kelley, and G. L. Rawley

We are developing thermometers based on the kinetic inductance of a superconducting meander strip.[6] The ultimate aim of this project is to obtain a working X-ray microcalorimeter which uses a kinetic inductance thermometer and to optimize its performance. Our prototype device consists of an aluminum meander strip and groundplane separated by a dielectric layer of SiO_2.

2. KINETIC INDUCTANCE THERMOMETRY

The energy stored in a magnetic field produced by a current I is

$$E = \frac{1}{2}L_M I^2 + \int_{\text{conductor}} \frac{1}{2} n m_q v^2 \, d\tau \equiv \frac{1}{2}L_M I^2 + \frac{1}{2}L_k I^2 \tag{1}$$

where

$$L_k = \left(\frac{m_q}{nq^2}\right)\left(\frac{l}{\sigma}\right) \tag{2}$$

L_k is the *kinetic inductance* of the circuit and depends on the geometry of the conductor through the length l and the cross-sectional area σ of the conductor. It also depends on the material through the number density n of the current carriers, their mass m_q, and their charge q.[7] In most situations L_k is negligible compared to L_M. However, for superconductors just below the critical temperature n becomes very small for Cooper pairs and L_k becomes very large. For a long thin superconductor with a groundplane and meanders to reduce L_M, L_k may dominate.

The inductance of a superconducting stripline is given by[8]

$$L = \mu_0 \frac{l}{w}\left[t + \lambda_s \coth\frac{d_s}{\lambda_s} + \lambda_g \coth\frac{d_g}{\lambda_g}\right] \tag{3}$$

where

$$\lambda_{g,s}(T) = \frac{\lambda_{g,s}(0)}{\sqrt{1 - \left(\frac{T}{T_c}\right)^4}} \tag{4}$$

is the penetration depth in the superconducting film. The subscripts g and s refer to the groundplane and meander strip, respectively. The length of the meander strip is l, w is its width, t is the thickness of the dielectric layer, and d_g and d_s are the thicknesses of the groundplane and meander strip as shown in Figure 1. The critical temperature is T_c and $\lambda(0)$ refers to the penetration depth at absolute zero. This function varies very rapidly with temperature close to T_c. There are two limiting cases which are of interest here. For thick films $d >> \lambda$ and $L_k \propto \lambda$. For thin films $d << \lambda$ and the temperature dependence is stronger: $L_k \propto \lambda^2$.

3. DEVICE FABRICATION

The meander strip and groundplane were patterned using a lift-off process.[9] A thick layer of photoresist was placed on the wafer and Al was deposited from vapor. The resist was then dissolved and its Al covering lifted off, leaving Al only on those parts of the wafer that had not been covered by resist. With this process there is no need to expose the device to strong etchants which might damage the dielectric layer.

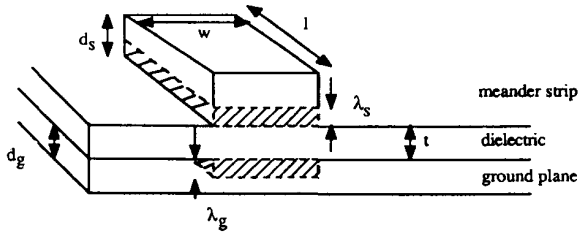

Fig. 1. Cross-section of a kinetic inductor. The supercurrents flow in the shaded regions.

The lift-off process is shown in Figure 2. The SiO_2 layer was chemically deposited and later etched to expose parts of the groundplane for bonding. The meander strip and groundplane are about 4000 Å thick. These values are much larger than the film thicknesses we hope to use eventually and were chosen to ensure reliable patterning and ease of bonding. The insulating SiO_2 layer is about 1100 Å thick. The meander is 7 cm long and 3.85 μm wide. The layout of the chip is shown in Figure 3.

4. TESTING

We observed the superconducting-normal transition of the meander strip with a current of 10 μA. The critical temperature was found to be 1.224 ± 0.006 K. As expected for a thin film, this is elevated slightly from the value for bulk aluminum which is 1.196 K.[10]

Meservey and Tedrow[7] have used a tunnel diode oscillator to measure kinetic inductance. We chose this readout method because of the oscillator's high stability and its ability to operate at liquid helium temperatures and also because of ease of implementation. We had intended to use a phase locked loop to measure the frequency but we found that a frequency counter was more convenient due to its greater dynamic range. The kinetic inductor was mounted in a T0-5 can on an aluminum stage along with a germanium resistance thermometer and a heating resistor. The stage was suspended on Kevlar threads from a supporting frame which held the tunnel diode oscillator. A thin copper strip connecting the stage to the frame was used to fine tune the thermal time constant of the stage. The frame was mounted on the cold stage of a ^{3}He dewar.

For kinetic inductance measurements the device was included in the tank circuit of the tunnel diode oscillator through superconducting niobium wires and the frequency was measured for different temperatures. The niobium wires were strung under tension to reduce microphonics. The setup is shown in Figure 4. It might seem simpler to have the kinetic inductor in series with L rather than C. However the present arrangement was chosen because the tunnel diode requires a dc bias current of about 30 μA which is greater than the critical current of some of the devices we have been testing.

Figure 5 shows how the oscillator frequency depends on temperature. As ex-

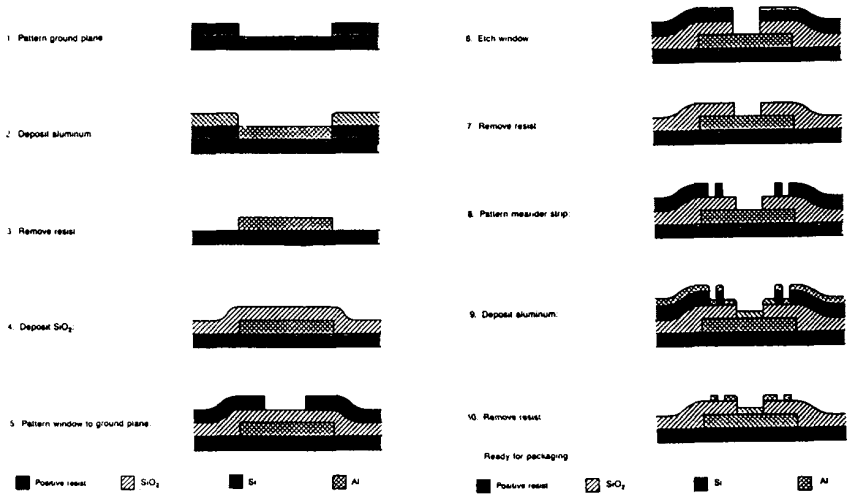

Fig. 2. Fabrication of the kinetic inductors.

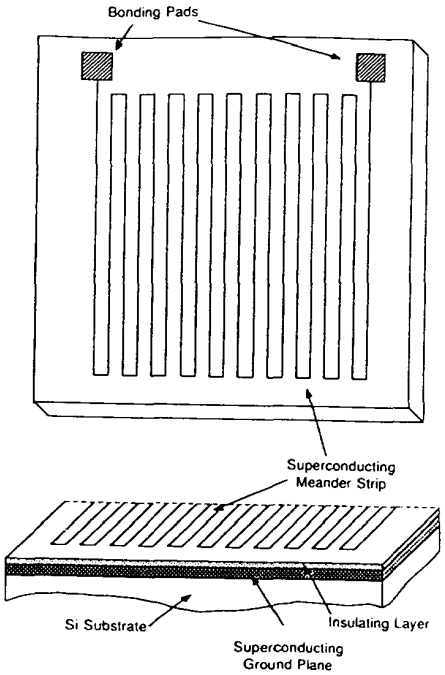

Fig. 3. Layout of the kinetic inductor.

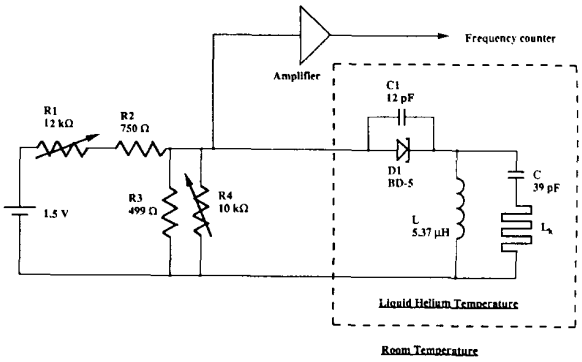

Fig. 4. The tunnel diode oscillator readout.

pected, the frequency drops sharply as T approaches T_c. The data were fitted to a function of the form

$$f = f_0\left(1 - f_0^2 \frac{\alpha}{\sqrt{1-(\frac{T}{T_c})^4}} \coth \beta\sqrt{1-(\frac{T}{T_c})^4}\right) \tag{5}$$

where

$$\alpha = \frac{4\pi^2 C^2}{(C+C_1)} \frac{\mu_0 l}{w} \lambda(0)$$

and

$$\beta = \frac{d}{\lambda(0)}$$

The frequency for $L_k = 0$ is f_0. Here we have taken the groundplane and meander strip to have equal T_c and $\lambda(0)$. This is reasonable since they were deposited by the same process and their thicknesses are approximately equal. From the device parameters we expect $\alpha = 1.3 \times 10^{-6}$ MHz^{-2} and $\beta = 8.3$ for $\lambda(0) = 480$ Å. The best fit values are $\alpha = (8.2 \pm 0.3) \times 10^{-7}$ MHz^{-2} and $\beta = 5.1 \pm 0.9$. the apparent diaagreement between the expected and measured values may be due to the fact that the large uncertainties in the temperature have not been taken into account.

Because the Al films are so thick, the kinetic inductance is found to be approximately proportional to the penetration depth.

5. Future Plans

Having successfully constructed a prototype kinetic inductance thermometer we intend to extend this technique to lower temperatures. The ultimate goal of this project is a monolithic X-ray microcalorimeter which operates at 0.1 K and uses a kinetic inductance thermometer. We plan to replace the tunnel diode oscillator readout with a D.C. SQUID and carry out detailed investigations of the noise to see if kinetic inductance thermometry can really provide better resolution than thermistors.

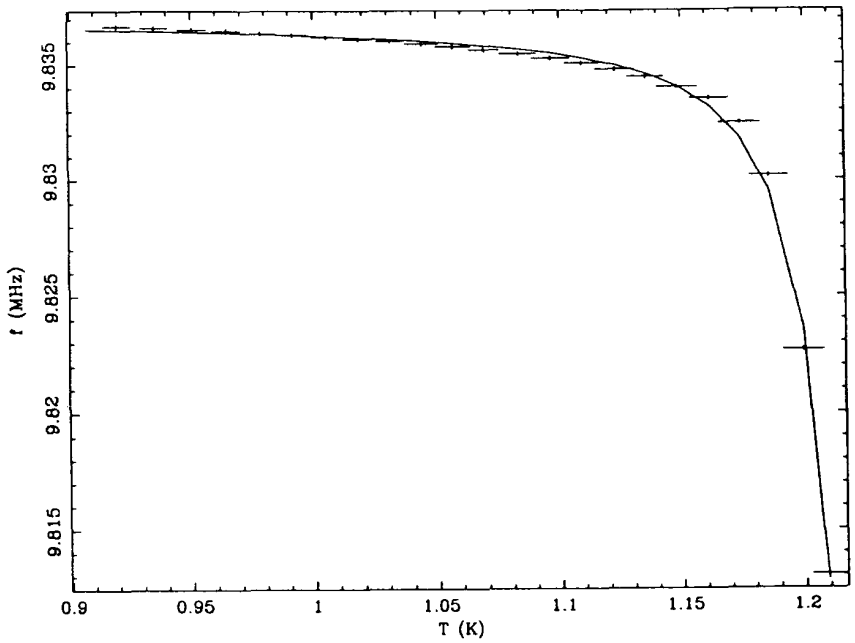

Fig. 5. Variation of TDO frequency with temperature.

ACKNOWLEDGMENTS

We wish to thank Harvey Moseley for useful suggestions and discussions. This research is supported by NASA grant NAG5-1176.

REFERENCES

1. P. J. Serlemitsos *et al.*, Frontiers of X-Ray Astronomy, ed. Y. Tanaka and K. Koyama, 221 (1992)
2. S.H. Moseley, J.C. Mather, and D. McCammon, J. Appl. Phys., 56, 1257 (1984)
3. D. McCammon *et al.*, Nucl. Phys., A527, 821c (1991)
4. D. G. McDonald, Appl. Phys. Lett., 50, 775 (1987)
5. J. E. Savageau and D. G. McDonald, IEEE Trans. Mag., MAG-25, 1331 (1989)
6. G. L. Rawley, R. L. Kelley, S. H. Moseley, and A. E. Szymkowiak, Proc. SPIE , 1159, 414 (1989)
7. R. Meservey and P.M. Tedrow, J. Appl. Phys., 40, 2028 (1969)
8. N. H. Meyers, Proc. IRE, 49, 1640 (1961)
9. M. Hatzatis, B. J. Canavello, and J. M. Shaw, IBM J. Res. Develop., 24, 452 (1980)
10. N. W. Ashcroft and N. D. Mermin, Solid State Physics, 729, Saunders College, Philadelphia (1976).

Signal Processing for Microcalorimeters

A. E. Szymkowiak, R. L. Kelley,
S. H. Moseley, and C. K. Stahle†

NASA / Goddard Space Flight Center, Greenbelt, MD 20771
†NAS / NRC Resident Research Associate at NASA / Goddard Space Flight Center

Most of the power in the signals from microcalorimeters occurs at relatively low frequencies. At these frequencies, typical amplifiers will have significant amounts of 1/f noise. Our laboratory systems can also suffer from pickup at several harmonics of the AC power line, and from microphonic pickup at frequencies that vary with the configuration of the apparatus. We have developed some optimal signal processing techniques in order to construct the best possible estimates of our pulse heights in the presence of these non-ideal effects. In addition to a discussion of our laboratory systems, we present our plans for providing this kind of signal processing in flight experiments.

We wish to produce accurate estimates of the energy of the x-rays incident on our microcalorimeters. With the current generation of devices and amplifiers we cannot obtain a sufficiently accurate estimate of pulse height from a sample taken at the peak of the signal. In addition, the variations from run to run in our measuring set-up and detectors would necessitate frequent re-tuning (or component changes) of any filtering scheme implemented in hardware. Thus we have focused on sampling the calorimeter signals and implementing the pulse height estimation as a digital filter.

Before discussing our filtering techniques, it is worthwhile to discuss when they can be profitably applied. Most of the signal power from our calorimeters occurs at relatively low frequencies (audio), which is unfortunate, since it is in this range where the combination of 1/f noise from the JFET amplifiers, pickup from the power line fundamental (and its multiples), and microphonic pickup from mechanical resonances are large enough to make filtering necessary. Conversely, it is fortunate that we operate at low frequencies, since it allows us to use relatively low cost digitizers in our attempts to deal with the noise sources mentioned above.

We assume that the pulses all have the same shape; that each pulse has the form

$$A \times S(t)$$

where A is the amplitude, and S(t) the pulse shape. Note that significant amounts of non-linearity can give rise to variations in pulse shape with the energy of the event. (This is to be distinguished from a non-linear gain (voltage of the signal per incident energy) which could be substantial without causing significant variations in pulse shape). The optimal pulse height estimate, H, is the one which minimizes (in the least square sense) the difference between the noisy data, D(t), and the model of the pulse shape. Here we transfer the expression to be minimized into the frequency domain;

$$x^2 = \sum \frac{\left[D(f) - H \times S(f)\right]^2}{N^2(f)}$$

where $N^2(f)$ is the power spectrum of the noise. Setting the derivative of this expression, to zero yields the optimal estimator of the pulse height as

$$H = \sum \frac{\left[D(f) \times S^*(f)\right]}{N^2(f)}$$

This expression can be transferred back into the time domain as

$$H = \sum D(t) \times F(t)$$

where, F(t), the optimal filtering template, is constructed by taking the inverse Fourier transform of $S(f)/N^2(f)$. Thus to construct the optimal filter we must accumulate the average pulse shape and the power spectrum of the noise.

If the power spectrum of the noise were "white" (constant), the optimal filter would be identical to the average pulse shape. Since our noise increases as we approach DC, our optimal filters typically have a region with negative weights before the pulse arrives. In effect, this region is measuring the height of the variable baseline, and subtracting it from the region under the pulse. Note that this means that we need information before the pulse arrives. If there are some peaks in the noise spectrum, due to pickup from the power line or from vibrations, the S/N ratio will be small at those frequencies, and the filter will effectively "notch out" the noise, regardless of its phase.

The x-rays arrive randomly, in particular with respect to the sampling. This fact increases the required sampling rate, even though there may not be significant amounts of signal power at high frequencies. As the arrival phase moves through the width of one sampling bin, the samples in each bin can change significantly, particularly where the voltage varies rapidly. There are several methods one can use to minimize the effects of this sampling phase error on the pulse height. One is to minimize the relative width of the sampling bins, by either sampling at very high frequencies, by limiting the signal bandwidth in the amplifier, or by removing the high frequency components from the filter template (since this can throw away signal power, the filter will no longer be "optimal"; although that optimality was defined for a constant pulse shape, and the presence of sampling phase error makes that assumption invalid). Another method is to solve for the arrival time, and correct the pulse height estimate. A third, similar method, is to fit a shape to the pulse height estimate obtained at several different lags, and interpolate to obtain the maximum height.

In the laboratory, we route the signal from an amplifier to a digitizing oscilloscope. We set the oscilloscope's triggering point so that a quarter or an eighth of the record will contain data from before the pulse. We usually AC couple the trigger, so that we will not be sensitive to drifts in offset, and set the triggering level just above the level of the noise. When the oscilloscope has captured a sweep, the data is transfered to a computer. Periodically the computer has the oscilloscope take a sweep without waiting for a trigger, to provide a measurement of the noise.

The recorded sweeps are transferred to a mainframe where we perform our filtering. First, we examine a few pulses to determine the regions over which we will measure the pulse risetime and the maximum height. A program measures these two quantities for all the records of the file, and we construct a scatter plot. Using this distribution, we pick a

range of these parameters which will be used to find "good" noise records, and pulses to use to construct the average pulse shape to be used during the filtering. Additionally, several parameters are set to reject records that contain more than one pulse. The filtering program then examines a subset of the file, applying the selection criteria in order to accumulate the average pulse shape and the power spectrum of the noise. These quantities are then used to construct the optimal filter template. In the next phase, the optimal template is convolved with each pulse record at a few lags. A pulse height is constructed from these convolutions, often by performing a parabolic fit to the pulse-height versus lag data. The risetime, pulse height, and lag are then output. We then make a plot of pulse height in a line versus time during the run to see if there are an discontinuities or trends from temperature changes during the run. We then can select regions from which to construct histograms.

Figure 1 is a plot from our optimal filtering program. The upper panel shows the average pulse shape, the middle panel the power spectrum of the noise, and the lower panel the optimal filter template. The ripples in the template are caused by the peak in the power spectrum of the noise at about 110 Hz.

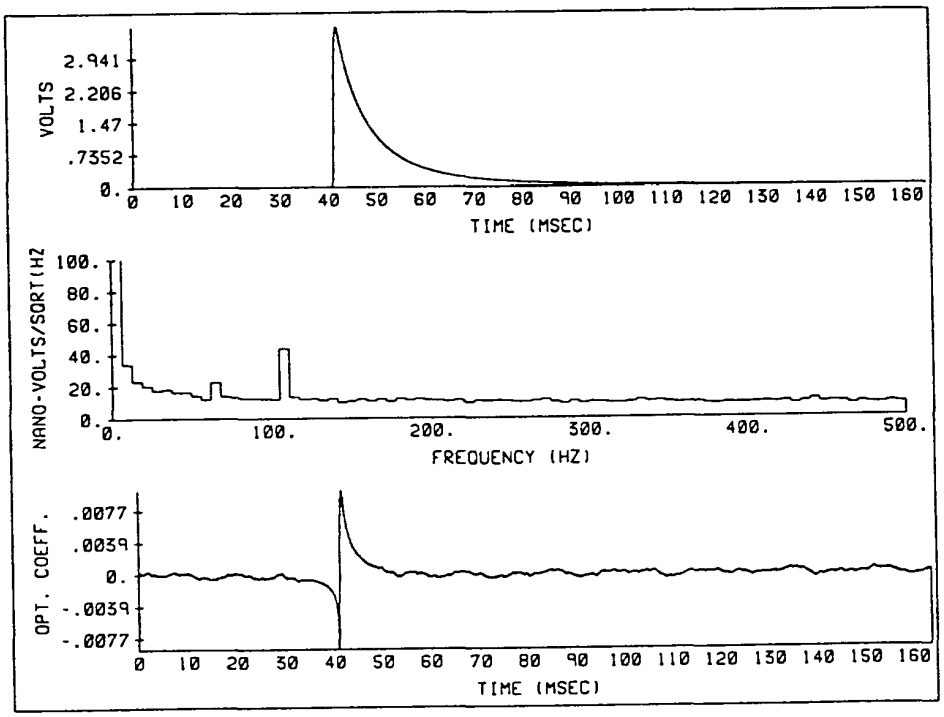

Fig. 1 Plots showing (top to bottom) average pulse shape, power spectrum of the noise, and the optimal filtering template.

Figure 2 is a further plot showing the power spectrum of the average pulse in the lower panel and the signal to noise ratio in the upper panel.

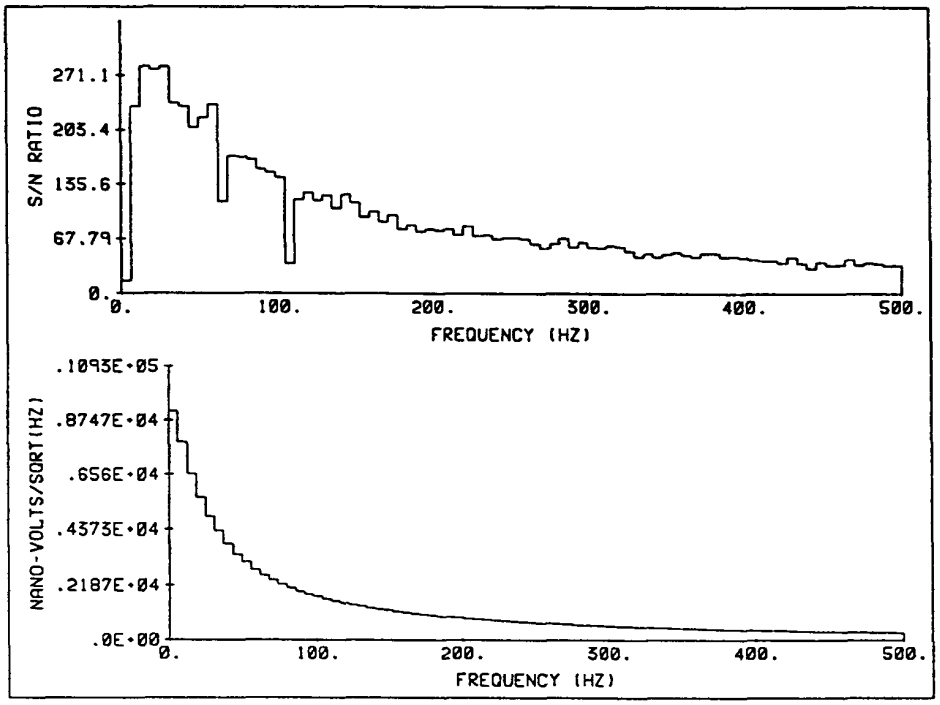

Fig. 2 Plots showing (top to bottom) signal to noise ratio and power spectrum of average pulse.

For our planned flight of a calorimeter array on a sounding rocket, we will have an adequate telemetry rate (1.6 megabits/sec) to operate in a mode simlar to that we use in our laboratory experiments; e.g. recording all the sweeps for later analysis. In addition to sending down the sampled sweeps, we will also telemeter down pulse heights determined by an on-board analog system. This second data stream was put in so that we will get frequent estimates of the gain of our system by tracking the shift of a line from an on-board radioactive source. This is to permit us to deal with rapid changes in temperature as the cryogenics recovers from heat inputs due to vibration during launch. The energy of the calibration line is larger than any celestial x-ray we expect during the flight, and we use this fact to discriminate against these events to avoid filling up the telemetry with sampled sweeps from these calibration events, while still having an adequate rate of these events to track the gain.

For a spacecraft instrument, it is unlikely that we would be able to have the bandwidth to send down the digitized waveforms, so we will have to perform the digital

filtering on-board. A number of digital signal processors (DSPs) are now available with the requisite capabilities needed to perform this filtering. These DSPs are microprocessors, with hardware to implement a multiply-accumulate operation in a single cycle, and usually several other optimizations for the types of operations required for signal processing. There are several schemes for using these DSPs. If resources permit, one scheme would use many DSPs, and no separate pulse detection circuitry. The DSP continuously examines the signal coming from an analog-to-digital converter (ADC), simultaneously storing the samples in a circular buffer. The DSP compares a continuously calculated, smoothed derivative with a threshold, to detect the arrival of a pulse. When a pulse is noted, the DSP fills the remainder of the circular buffer, and then convolves the stored "sweep" with a template. The pulse height estimate, along with a time tag and some flags, would then be telemetered to the ground. In other schemes, hardware threshold detection is used with an autonomous buffer, and a DSP, serving many channels, is only invoked to perform the convolutions,

We have built a breadboard using candidate ADCs and DSPs. We have chosen some ADCs that have become available to support the digital audio market. These ADCs, using the sigma-delta conversion technique, take low-resolution samples at a very high rate and use an internal digital filter to construct the lower rate, high-resolution outputs. This technique avoids the requirement for external anti-aliasing filters with a sharp, high-frequency cut-off, and reduces the complexity of the circuitry for each channel.

Tests with our breadboard have shown that such a system has the requistite capability to perform the pulse height estimation. We are evaluating additional candidate DSPs, and should soon be choosing the digital filtering components for our spectrometer on NASA's Advanced X-ray Astrophysics Facility.

ACKNOWLEDGEMENTS

We thank Robert Baker for designing the breadboard system and for the initial programming of the DSP. We also thank Tim Stowe for his efforts in further improving the DSP filtering programs

THE X-RAY SPECTROMETER (XRS) INSTRUMENT FOR THE AXAF-S MISSION

Greg Madejski, Stephen S. Holt, Richard Kelley, S. Harvey Moseley, Caroline Stahle, Andrew Szymkowiak (NASA/Goddard), and

Dan McCammon, Michael Juda, and Jiahong Zhang (University of Wisconsin)

ABSTRACT

The recent restructuring of the Advanced X-ray Astrophysics Facility (AXAF) program resulted in two separate spacecraft, AXAF-S, for high throughput, high energy resolution X-ray spectroscopy, and AXAF-I, devoted to high spatial resolution X-ray imaging. The focal plane instrument of AXAF-S is the X-ray Spectrometer (XRS). In this paper, we discuss the rationale for astrophysical X-ray spectroscopy and describe the XRS instrument, which is a microcalorimeter capable of precise measurement of the energy of incoming individual X-rays with high efficiency.

Motivation for High Resolution Astrophysical X-ray Spectroscopy

X-ray astronomy is a relatively new science: it originated in the 1960s with a rocket flight, which revealed the existence of celestial X-ray emitters. Subsequent satellite-borne instruments discovered that X-ray emission is a property of a wide variety of objects in the sky: single stars, binary stellar systems, supernova remnants, galaxies, clusters of galaxies and active galactic nuclei. In all cases, the X-ray fluxes are modest, less than 1 photon/sec/cm^2, and thus large collecting area and high efficiency are particularly important design goals for any sensitive X-ray detector.

Most of the early X-ray detectors were essentially large proportional counters, collimated to receive the X-rays from only one direction in the sky. However, since such instruments are also sensitive to energetic particles present in the near-Earth environment, the non-X-ray background can easily contaminate the data for celestial X-ray sources. The best approach to minimize the background, and thus substantially improve the sensitivity, is to focus X-rays into a small area. On one hand, focussing produces an image, which often has useful information in it (for instance, for the study of the spatial structure of diffuse X-ray sources such as hot matter ejected from a supernova explosion or hot gas in a cluster of galaxies). On the other hand, since the background is usually roughly proportional to the volume of the detector, this can yield tremendous (several orders of magnitude) reduction in background. Most modern X-ray mirrors reflect X-rays via grazing incidence, and are capable of resolving sources that are of the order of an arc second apart (as is, for instance, the case for the AXAF-I mirror). The mirrors considered for AXAF-S are extensively discussed in other papers at this conference, but the expected spatial resolving power of mirrors under consideration for AXAF-S is of the order of 1 arc minute.

It was clear from even the early missions that X-ray spectra of the celestial objects are complex and diverse, and carry a tremendous amount of information. In general, X-rays are emitted by matter that is highly energized: either hot gas, of order of several million degrees Kelvin, or by very fast electrons rapidly loosing their kinetic energy. The overall shape is usually indicative of the basic physical process; a spectrum produced by a hot black body (for instance, due to dense, opaque gas) will have a shape of the Planck curve, while that produced by energetic electrons spiraling in a magnetic field is likely to exhibit a power law form. Importantly, in a similarity to the optical spectroscopy, electron

transitions in individual elements produce radiation at characteristic energies ("lines"). A precise study of strength of these lines can yield information about the relative elemental abundances and ionization stages of the radiating matter. The relative strengths of the lines should yield temperature and density. The width of the lines, usually due to Doppler-broadening, should give further clues as to the temperature, but importantly, is also a tracer of the bulk motion (kinematics) of the emitting matter.

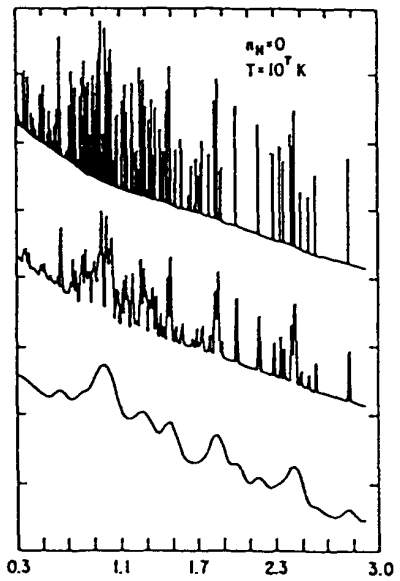

Figure 1. Spectrum of an astrophysical plasma with temperature of 10^7 K, as measured with detectors of energy resolution 1 eV (top), 10 eV (middle), and 100 eV (bottom). (From ref. 1).

Proportional counters rely on conversion of an X-ray energy to charge pairs, and thus their energy resolution (defined as $\Delta E(FWHM)/E$) is fundamentally limited to no better than ~ 15%. As a result, only the overall spectral shape of the source of X-rays could be determined from data obtained with them. That is enough to make general inferences about the temperature of gas radiating in clusters of galaxies, or distinguish between a thermal or non-thermal processes in supernova remnants. However, such modest $\Delta E/E$ was not quite sufficient to determine the relative abundances of heavy elements in clusters of galaxies to clearly determine if the intra-cluster gas is matter enriched in heavy elements, and thus ejected or stripped from the member galaxies, or if that matter is primarily hydrogen, implying that the cluster formed first, and the individual galaxies coalesced from that matter. While the proportional counter data implied that heavy elements are indeed present in clusters (ref. 2), at least an order of magnitude better spectral resolving power was needed to provide the detailed answers. To illustrate the expected richness of a spectrum for an astrophysical source, Fig. 1 shows a 0.3 - 3 keV spectrum of collisionally-dominated plasma, of similar kind that is found in supernovae, as observed with detectors with energy resolution FWHM of 1, 10, and 100 eV (for details, see ref. 3).

The first step in the direction of better spectral resolution was provided by the use of solid state detectors, pioneered by our own Solid-State Spectrometer flown on the *Einstein* Observatory (ref. 4). Further improvement (including the extension of the bandpass to 0.3 - 10 keV, and thus including the crucial iron K line region at ~ 6 - 7 keV) came in the Shuttle-based Broad-Band X-ray Telescope, where the solid state detector featured the energy resolution of ~ 100 eV, an improvement by about a factor of 4 - 5 as compared to proportional counters (ref. 5). The observations from that brief mission have produced tremendous wealth of data, showing, among other things, that the gas in clusters of galaxies has elemental abundances of ~ 1/2 Solar, and the redshift (and thus distance) of that gas is almost exactly that of the member galaxies as measured using optical techniques (ref. 6). They thus proved that X-ray spectroscopy can be used as an independent distance measurement to distant clusters. They also showed that the soft X-ray emission from Seyfert 2 galaxies is dominated by emission lines, presumably due to K and L shell transitions of oxygen and iron (ref. 7).

Importantly, the BBXRT data showed that it is essential to have better energy resolution for a detailed study of these lines. That is because the important region around 1 keV contains many lines from various elements, separated only by less than 50 eV, which, when observed with the BBXRT energy resolution, blend together into a single emission feature. Preliminary results from the joint Japanese - US X-ray astronomy satellite ASCA, featuring silicon charge-coupled devices as X-ray detectors, confirm that need.

Another example where the improvement in energy resolution is essential to further our understanding is the structure of Active Galactic Nuclei. These objects are extremely luminous, and thus can be observed at very large distances, making them good tracers of the large structure of the Universe. They are thought to be powered by infall of interstellar matter onto a compact central object, most likely a massive (more than a million Solar masses) black hole. However, a definite proof that black holes are present in these objects requires, among other things, kinematical proofs that the matter is indeed accelerating under the strong influence of the expected intense gravitational field. In such proximity to the central source, the matter is generally strongly ionized, and thus optical studies (where high spectral resolution is available from the ground) are not possible; the best tracers of this matter are fluorescence lines produced by the incident X-ray radiation. The best candidate lines are K transitions in iron; that is because the fluorescent yield quickly increases with the atomic number Z, yet the relative abundance, generally decreasing with Z, is still sufficiently high for iron to produce a strong emission line. In such a strong field the iron K line emitted by the infalling gas - normally expected to occur in the 6 - 7 keV energy range - should be Doppler-broadened in a well-defined fashion (ref. 8). However, the energy resolution of solid state detectors at 6 keV is generally insufficient for such a study, and grating instruments or Bragg crystal instruments have very little or no sensitivity in that energy range.

It is therefore clear that understanding the details of the physics responsible for the radiative processes requires substantially improved spectral resolution. A good quantitative example is the determination of the density and temperature of the hot gas in supernova remnants. While it is possible to measure a product of density and temperature from observations with lower energy resolution detectors, to determine these quantities separately, one must resolve and separately measure the strengths of the resonance, forbidden and intercombination lines from the helium-like state of a single element of the emitting gas. For oxygen, silicon, and iron, energy resolution of at least 15 eV is required to resolve these lines (ref. 1). Most importantly, since an improvement of energy resolution, for a given source, results in fewer photons in each energy bin, it is crucial that whatever instrument is used for observation, it must be highly efficient, and capable of observing the entire energy range simultaneously (ref. 1). The ultimate goal of astrophysical X-ray spectroscopy is thus to maximize both the energy resolution of the instrument, and the number of photons per energy resolution element.

The X-ray Spectrometer for AXAF-S

The quantum X-ray microcalorimeter, the focal plane instrument for AXAF-S, appears to be the best current solution to meet this goal. The detector has been invented and developed at our lab at NASA/Goddard jointly with the University of Wisconsin (ref. 9, 10), but there are other groups (among others, at Lawrence Livermore National Labs), that are developing similar instruments. The detector is capable of measuring the energy of incoming X-ray photons simultaneously over a broad range of energies, ~ 0.4 to 10 keV, at an unprecedented energy resolution of 12 eV. Its

efficiency is *nearly unity simultaneously over the entire bandpass*, which is about an order of magnitude better than dispersive instruments, which rely on transmission or reflection of X-rays from a grating. The determination of the energy of the incident photon is accomplished via the measurement of the temperature rise ΔT (assumed to be much smaller than the heat sink temperature T) associated with its absorption. Schematically, the detector is illustrated in Fig. 2; it consists of a silicon structure with an implanted thermometer, with an X-ray absorber attached to it. The structure is connected to a thermal heat sink by a thermal link of thermal conductance G. If the heat capacity of the detector is C, then absorption of a photon with energy E_p results in ΔT given by

$$\Delta T = E_p/C,$$

and the detector returns to the heat sink temperature with a time constant

$$\tau = C/G.$$

The fundamental noise limit of the detector is due to the random transport of phonons between the detector and the thermal bath in the thermal link connecting them. For a detector of heat capacity C, operating at the bath (heat sink) temperature T, the limiting FWHM energy resolution is (refs. 9, 10)

$$\Delta E = 2.35\ \xi\ (k\ T^2\ C)^{1/2},$$

where k is the Boltzman's constant. The variable ξ is of the order of 2, and is dependent on the design of the thermometer.

The energy resolution of the detector increases with decreasing heat capacity of the materials chosen for the substrate and for the absorber, and thus one of the challenges of the design is to find material of lowest possible heat capacity that would be sufficiently opaque to X-rays. Many materials, including silicon, the material used for the detector structure, have extremely low heat capacities at low temperatures. However, silicon is not suitable for X-ray absorption, since the large electronic bandgap allows many long-lived trap sites for the electrons, precluding rapid and efficient conversion of the X-ray to thermal energy, and thus a separate absorber is needed.

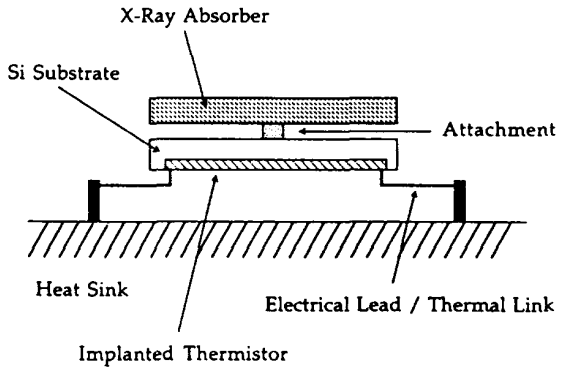

Figure 2. Schematic of a microcalorimeter. The X-ray is absorbed and its energy converted to heat in the absorber. The heat flows through the attachment into the silicon detector substrate. The temperature rise of the detector is sensed by a thermometer, which is connected to the external amplifier using electrical connections in the thermal links. The detector returns to equilibrium as the heat from the event flows to the heat sink through the thermal links. (From ref. 11.)

The desired size of the detector is determined by the characteristics of the mirror used for focussing X-rays. In the case of AXAF-S, the imaged size of a point source is about 1 arc min, which, with the focal length of ~ 4 meters, indicates that a detector with elements of ~ 0.25 mm^2 would be appropriate. Since the heat capacity of the absorber - and thus resulting energy resolution - drops with the detector operating temperature, the required energy resolution (~ 12 eV FWHM) and the required detector size imply that the operating temperature must be about 0.1 K. Such temperatures are achievable via cryogenic techniques, with the use of liquid helium as the first stage, and the additional sub-cooling via other means. While developing a flightworthy

refrigerator is an important challenge, helium dewars have been previously flown on several occasions, and proved reliable in space. The sub-cooling will be accomplished via the use of an adiabatic demagnetization refrigerator (see, e.g., ref. 12), where a paramagnetic salt is magnetized while thermally connected to the cryogen, and then isolated, and allowed to demagnetize, thus absorbing heat from the detectors. The flight-like version has been constructed at Goddard (ref. 13), and is capable of maintaining the detectors at below 0.1 K for several hours; a schematic of it is illustrated in Fig. 3. Temperature regulation at the desired level (typically better than 50 microKelvin) is accomplished by adjusting the magnetic field via a feedback loop, while the "recharge" of the refrigerator, typically lasting ~ 20 minutes, can be done while the observed astrophysical target is behind the Earth.

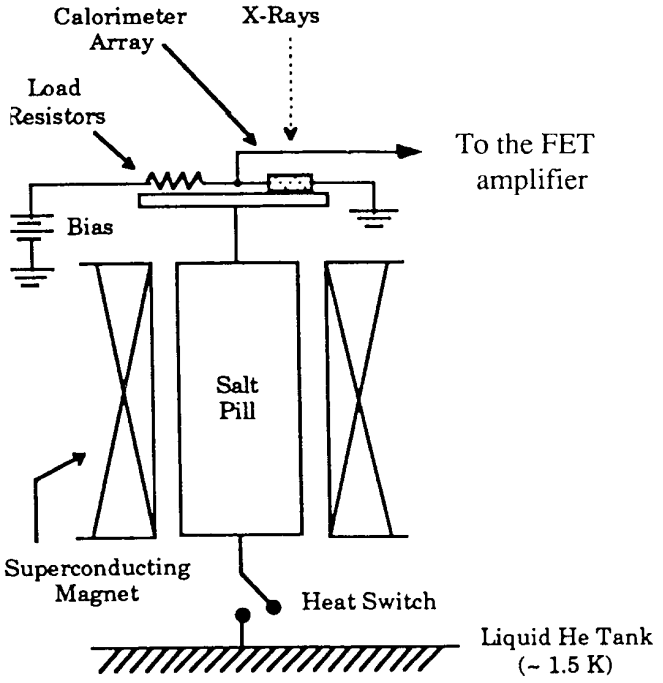

Figure 3. Schematic of the XRS, which consists of the adiabatic demagnetization refrigerator with its associated heat switch, and the detector assembly with the associated first stage FET amplifier.

The main challenge of the detector design, in addition to the minimization of the heat capacity, is the design of the thermometer capable of sensing the detector temperature with the lowest possible noise, yet maintaining a reasonably high degree of linearity. The thermometers in the detectors developed at Goddard are resistive, operating on the principle of phonon-assisted electron hopping conduction, where the conductivity rises rapidly with an increase in temperature. In such a thermometer (ref. 9, 10) the resistance R depends on temperature T such that

$$R = R_0 \exp ((T_0/T)^{1/2}).$$

These thermometers are ion-implanted into the monolithic silicon structure, and the contacts to the thermometer are brought out by degenerately doped traces. The thermometer is a part of a voltage divider, and thus the increase in the temperature will appear as a change of voltage accross it; the schematic of the calorimeter circuit is included in Fig. 3. Typically, the thermometers have a resistance of the order of 10 - 50 MΩ, to match to the input impedance of a JFET source follower amplifier. The details of the design optimization focus on the fact that on one hand, the thermometer has a larger specific heat than the surrounding silicon, and thus a small volume would be preferred; on the other hand, a smaller thermometer volume results in an increase of the current noise, as well as departure from the R (T) function given above, which reduces sensitivity of the thermometer. While our current design is compatible with the energy resolution requirements, detailed study should yield further improvements. Our current baseline detector consists of 3 rows of 12 detectors, each detector at 0.25 mm x 1 mm, and is illustrated in Fig. 4. Each detector in this arrangement is small enough to meet the energy resolution requirement, yet the entire array covers the spot size in the focal plane of AXAF-S adequately, and even allows for some moderate spatial information.

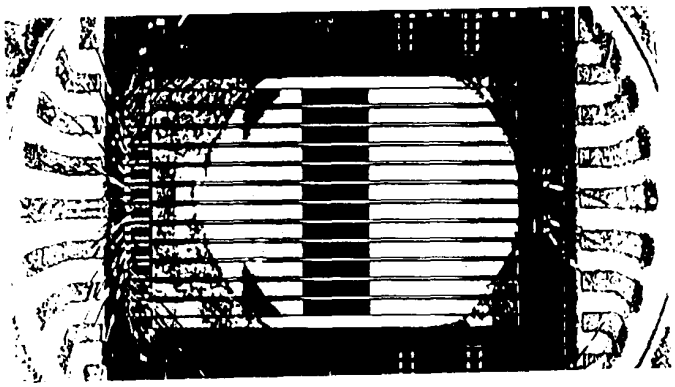

Figure 4. Photograph of one row of 12 detector elements for the XRS, without the absorbers attached. The current baseline includes an assembly of 3 such rows, where the 4 corner elements will not be used. Each element is 0.25 mm x 1 mm, and will be covered by absorber attached to it; the current absorber material is a 12 μm thick piece of mercury telluride (HgTe).

Another challenge lies in the choice of suitable absorber. As mentioned previously, the large bandgap renders silicon unsuitable. The absorber has to absorb and thermalize the incident X-ray energy efficiently and rapidly while having the lowest possible heat capacity; absorption increases with the atomic number. Our current baseline absorber is mercury telluride, a semiconductor with nearly-zero bandgap. To stop 99% of 6 keV X-rays, a thickness of 12 μm of HgTe is required. Our tests showed that the energy resolution of a good detector with HgTe absorber of dimensions of 12 μm x 0.25 mm x 1 mm is 11.5 eV. Fig. 5 shows the spectrum from one detector element, obtained by illuminating it with a ^{55}Fe radioactive X-ray source, producing ^{55}Mn lines at ~ 5.9 keV.

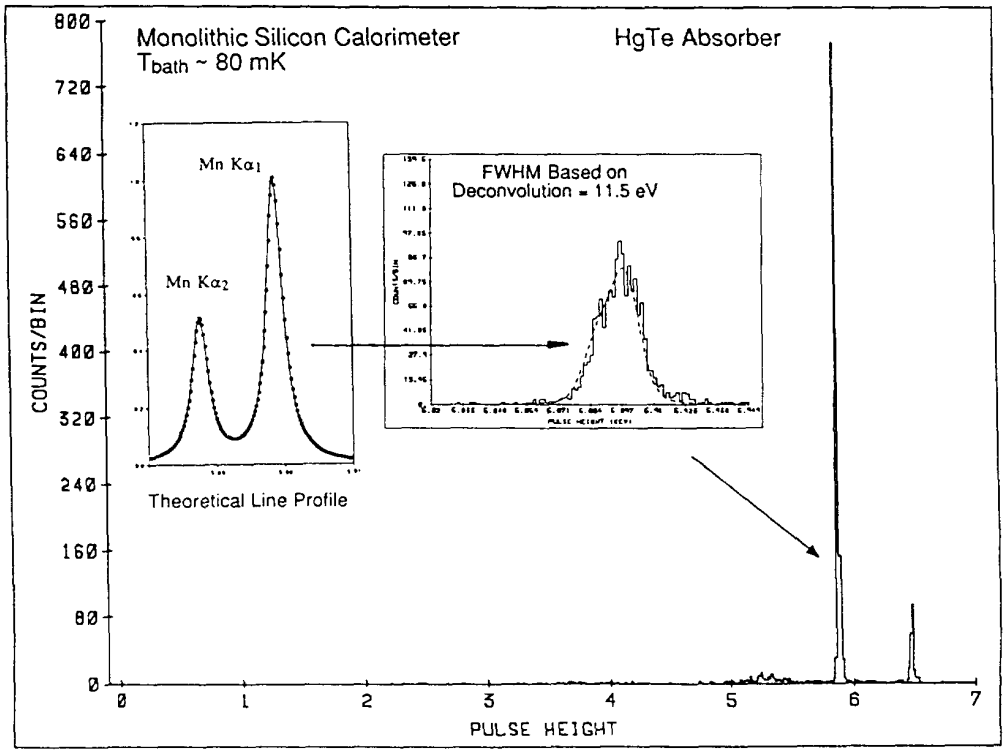

Figure 5. The spectrum of ^{55}Mn X-rays measured with one element of our baseline detector. The energy resolution was determined by convloving the line profile (inset) with a Gaussian until a good fit was obtained. The derived energy resolution is 11.5 eV (FWHM). (From ref. 11.)

The main limitation of the small bandgap semiconductor absorbers is that they tend to have large heat capacity. Further improvement in the heat capacity of the absorber should be available from the use of superconductors. Below the transition temperature, the heat capacity of superconductors is very low, as it is solely due to the lattice; the electrons are in their superconducting ground state, and do not contribute appreciably, unlike normal metals, in which electrons dominate the heat capacity. We evaluated a variety of superconductors, and found that tin is so far the most promising (ref. 11). Despite problems in thermalization due to the process of excited electrons recombining into Cooper pairs, with the use of tin absorbers, we have obtained energy resolution comparable to that using HgTe. Since superconductors show great promise as absorbers, we continue to study their X-ray thermalization properties.

In summary, the X-ray Spectrometer, to be flown at the turn of the century aboard the AXAF-S mission, will open a new "discovery space" in X-ray astrophysics. It will afford a very good spectral resolution of 12 eV over a wide bandpass, ~ 0.4 to 10 keV. This capability will permit an unprecedented sensitive study of a wide range of astrophysical sources, hopefully both answering many of the outstanding questions in astrophysics, and posing many new questions for generations to come.

References

(1) Holt, S. S. 1991, in *Iron Line Diagnostics in X-ray Sources*, Lecture Notes in Physics **385**, eds. A. Treves, G. C. Perola, and L. Stella (Berlin : Springer-Verlag), 289.

(2) Serlemitsos, P., Smith, B. W., Boldt, E. A., Holt, S. S., and Swank, J. H. 1977, *Ap. J. (Lett.)*, **211**, L63.

(3) McCammon, D., and Sanders, W. T. 1990, *Ann Rev. Astron. Astrophys.*, **28**, 657.

(4) Holt, S., *et al.* 1979, *Ap. J. (Lett.)* **234**, L65.

(5) Serlemitsos, P. J., *et al.* 1992, in *Frontiers of X-ray Astronomy*, **FSS-2**, eds. Y. Tanaka and K. Koyama, (Tokyo : Universal Academy Press), 221.

(6) Arnaud, K. A., *et al.* 1992, in *Frontiers of X-ray Astronomy*, **FSS-2**, eds. Y. Tanaka and K. Koyama, (Tokyo : Universal Academy Press), 481.

(7) Marshall, F. *et al.* 1992, in *Frontiers of X-ray Astronomy*, **FSS-2**, eds. Y. Tanaka and K. Koyama, (Tokyo : Universal Academy Press), 233.

(8) Stella, L., and Campana, S. 1991, in *Iron Line Diagnostics in X-ray Sources*, Lecture Notes in Physics **385**, eds. A. Treves, G. Perola, and L. Stella (Berlin : Springer-Verlag), 230.

(9) Moseley, S. H., Mather, J. C., and McCammon, D. 1984, *J. Appl. Phys.*, **56**, 1257.

(10) Moseley, S. H., Kelley, R., Mather, J., Mushotzky, R. F., Szymkowiak, A. E., and McCammon, D. 1985, *IEEE Trans. Nucl.Sci.* **NS-32**, 134.

(11) Moseley, S. H., Juda, M., Kelley, R. L., McCammon, D., Stahle, C. K., Szymkowiak, A. E., and Zhang, J. 1992, *Proc ESA Symp. on Photon Detectors for Space Instrumentation*, **ESA SP-356**, 13.

(12) Kelley, R. L., Holt, S. S., Madejski, G. M., Moseley, S. H., Schoelkopf, R. J., Szymkowiak, A. E., McCammon, D., Edwards, B., Juda, M., Skinner, M., and Zhang, J. 1988, in *X-ray Instrumentation in Astronomy II*, ed. L. Golub, Proc. SPIE **982**, 219.

(13) Serlemitsos, A. 1992, *Cryogenics*, **32, No.2**, 117.